A "Trimer of Dimers"—Based Model for the Chemotactic Signal Transduction Network in Bacterial Chemotaxis

Xiangrong Xin & Hans G. Othmer

Volume 75 • Number 1
January 2013

Bulletin of Mathematical Biology

A Journal Devoted to Research at the Junction of Computational, Theoretical, and Experimental Biology

Society for Mathematical Biology

≜ Springer

Online First
Immediately Online
www.springerlink.com

Faster publication!

≜ Springer

Springer

ORIGINAL ARTICLE

A "Trimer of Dimers"—Based Model for the Chemotactic Signal Transduction Network in Bacterial Chemotaxis

Xiangrong Xin · Hans G. Othmer

Abstract The network that controls chemotaxis in *Escherichia coli* is one of the most completely characterized signal transduction systems to date. Receptor clustering accounts for characteristics such as high sensitivity, precise adaptation over a wide dynamic range of ligand concentrations, and robustness to variations in the amounts of intracellular proteins. To gain insights into the structure-function relationship of receptor clusters and understand the mechanism behind the high-performance signaling, we develop and analyze a model for a single trimer of dimers. This new model extends an earlier model (Spiro et al. in Proc. Natl. Acad. Sci. 94:7263–7268, 1997) to incorporate the recent experimental findings that the core structure of receptor clusters is the trimer of receptor dimers. We show that the model can reproduce most of the experimentally-observed behaviors, including excitation, adaptation, high sensitivity, and robustness to parameter variations. In addition, the model makes a number of new predictions as to how the adaptation time varies with the expression level of various proteins involved in signal transduction. Our results provide a more mechanistically-based description of the structure-function relationship for the signaling system, and show the key role of the interaction among dimer members of the trimer in the chemotactic response of cells.

Keywords *E. coli* · Adaptation · Robustness · Sensitivity

1 Introduction

In response to environmental signals such as light, temperature, or chemicals, motile organisms can change their behavior by directed movement toward or away from the

X. Xin
Department of Biomedical Engineering, University of Minnesota, Minneapolis, MN 55455, USA

H.G. Othmer (✉)
School of Mathematics and Digital Technology Center, University of Minnesota, Minneapolis, MN 55455, USA
e-mail: othmer@math.umn.edu

signal, which is called *taxis*, by changing their speed of movement and/or frequency of turning, which is called *kinesis*, or by a combination of these.[1] *E. coli* employs kinesis to move in a favorable direction, and in particular, it executes the "bakery walk" in finding a favorable location, which is to take a "sniff" and judge the signal intensity at the present location, take a "step" and another sniff, compare the signals, and from the comparison decide on the next step. In this process, it alternates between a more or less linear motion called running (the "step") and a highly erratic motion called tumbling, which produces little translocation but reorients the cell. *E. coli* has 6–8 motor-driven flagella that can rotate in either direction, and when they rotate counterclockwise (CCW) when viewed from behind they form a bundle that propels the cell forward in a run, but when they rotate clockwise (CW) the bundle flies apart and the cell tumbles. Since these bacteria are 1–2 μm in length, they are too small to detect spatial differences in an extracellular signal on the scale of a cell length, and they choose a new direction essentially at random at the end of a tumble, although it has some bias in the direction of the preceding run (Berg and Brown 1972). In the absence of a signal the run times are much longer than the tumbling times, and when bacteria move in a favorable direction (i.e., either in the direction of foodstuffs or away from noxious substances), the run times are increased further by increasing the probability p(CCW) of CCW rotation (called the rotational bias) (Berg and Brown 1972; Berg and Tedesco 1975; Larsen et al. 1974; Silverman and Simon 1974; Spudich and Koshland 1975; Stock et al. 1991). The effect of alternating these two modes of behavior is that a bacterium executes a three-dimensional random walk with drift in the favorable direction, when observed on a sufficiently long time scale (Berg 1975; Koshland 1980). In addition, *E. coli* adapts to constant signal levels and only alters the run length in response to changes in the extracellular signals; in effect the sensory system functions as a derivative detector. Thus, chemotaxis comprises two essential phases: *excitation* that leads to a change in the tumbling rate, and *adaptation*. The former is fast—it occurs in a fraction of a second in response to a step change in the signal—while the latter is slow, and takes from seconds to minutes depending on the size of the stimulus (Block et al. 1982; Stock 1994).

The signal transduction system that underlies *E. coli* chemotaxis involves five dimeric membrane-spanning chemoreceptors (Tsr, Tar, Tap, Trg, and Aer), which are members of a family of transmembrane methyl-accepting chemotaxis proteins (MCPs), and six intracellular Che proteins (CheA, CheW, CheY, CheZ, CheR, and CheB). Tsr and Tar are the major receptors with a few thousand copies per cell; Tap, Trg, and Aer are minor types with a few hundred copies per cell. Two central components are the histidine kinase CheA, which autophosphorylates, and the motor regulator CheY, to which the phosphorylated CheA transfers its phosphoryl group. CheA and the adapter protein CheW bind to receptors to form a stable ternary signaling complex, and when an extracellular signal binds to receptor sites on the complex, the autophosphorylation rate of CheA is modulated. $CheA_p$ transfers the phosphoryl group to CheY, which then diffuses to the flagellar motors. When $CheY_p$ binds to the

---

[1]Usually the distinction between taxis and kinesis is ignored, and we follow this convention here, and refer to the process as chemotaxis when the signal is a chemical.

protein FliM at the base of a motor, it increases the probability p(CW) of CW rotation, and thus increases the tumbling rate. The phosphatase CheZ reduces the CW signal by catalyzing the dephosphorylation of $CheY_p$. Attractant binding to or repellent release from the receptors inhibits the kinase activity of CheA, and thereby decreases the intracellular $CheY_p$ level and increases the run time, whereas decreases in attractants or increases in repellents function oppositely. Thus, the excitation response to a favorable signal consists of a rapid decrease in the activity of the kinase, a decrease in the level of $CheY_p$, and a decrease in the probability of tumbling, all on the time scale of a few hundred milliseconds (Bourret and Stock 2002).

Adaptation to chemotactic signals arises as follows. In addition to their extracellular ligand binding domain, chemoreceptors also have four or more sites in the cytoplasmic domain that are occupied either by glutamine (Q) or glutamate (E). Glutamate is methylated by the methyltransferase CheR ($E \rightarrow E_M$) and demethylated by the methylesterase $CheB_p$ ($E_M \rightarrow E$), and glutamine is also deamidated to glutamate ($Q \rightarrow E$) by $CheB_p$. In addition to the effect of ligand binding, the kinase activity of CheA is also controlled by the methylation level of receptors; addition of a methyl group increases the activity and vice versa. CheR is unregulated, whereas the activity of CheB increases significantly when it is phosphorylated by $CheA_p$, and when kinase activity is high it leads to a lower methylation level, and thus functions as a negative feedback in the transduction pathway. Thus, the overall response to an attractant can be summarized as a rapid decrease in kinase activity and $CheY_p$, followed by a slower restoration of the kinase activity due to methylation of occupied receptors.

E. coli can sense and adapt to ligand concentrations spanning more than five orders of magnitude, and can detect a change in occupancy of the aspartate receptor Tar as small as 0.1–0.2 %, which corresponds to the binding of one or two ligand molecules per cell (Bourret et al. 1991). If we define the gain in signal transduction as the change in rotational bias divided by the change in receptor occupancy, the gain can be as high as 55 (Segall et al. 1986). If we define the upstream signaling gain as the ratio of the relative change in kinase activity divided by the change in receptor occupancy, it is up to 35 (Sourjik and Berg 2002a). Most of the MCPs associate with CheA and CheW, and the ternary signaling complexes aggregate into heterogeneous clusters predominantly localized at one cell pole (Maddock and Shapiro 1993; Kim et al. 1999; Ames et al. 2002; Studdert and Parkinson 2004, 2005). Cooperativity in ligand binding and activity regulation induced by receptor clustering and interaction contributes to the high sensitivity (Bray et al. 1998; Shi and Duke 1998; Duke and Bray 1999; Sourjik and Berg 2004), but it is not clear whether long-range spatial interactions between receptors play an essential role in the high gain; some models rely on it, but we show that much of the data can be explained without invoking interactions beyond the level of trimers.

Models that invoke receptor clustering fall into two categories: in one category, receptors exist in a large, extended weakly-coupled network and conformational changes spread from ligand-bound receptors to neighbors through protein-protein interactions, and these can be formulated as a classical Ising model (Shi and Duke 1998; Duke and Bray 1999; Shimizu et al. 2003; Mello and Tu 2003; Mello et al. 2004). In the other, it is assumed that receptors exist in smaller but

more strongly coupled clusters and simultaneously flip between active and inactive states, and these can be thought of as a classical Monod–Wyman–Changeux (MWC) model (Sourjik and Berg 2004; Mello and Tu 2005; Keymer et al. 2006; Endres and Wingreen 2006). Both Ising-type and MWC-type models treat the receptor dimer as the basic functional unit and thus receptor interactions are at the dimer-dimer level. However, it is now well established that the basic functional unit is a trimer comprised of three tightly-linked receptor dimers that a large number of trimers are loosely-arranged in an hexagonal array (Khursigara et al. 2008; Briegel et al. 2008), and that a trimer of dimers has greater kinase activation than either a single dimer or a multiple-trimer cluster (Boldog et al. 2006). All the data suggest that structurally and functionally, the trimer of dimers is the core unit of receptor clusters. Thus, it is likely that the short-range interaction between dimers within a trimer is the primary determinant of signal transduction, and that the long-range interaction between trimers is secondary. This is supported by the observation that the extremely high cooperativity of receptors (a Hill coefficient for the kinase activity response larger than 3) is only observed in two special cases: responses by the *cheRcheB* mutant cells with Tar or Tsr highly over-expressed (Sourjik and Berg 2004), or by the receptor Tsr *in vitro* (Li and Weis 2000), while in wild-type cells and other *cheRcheB* mutant strains, the cooperativity is more moderate (the Hill coefficient is less than 3). A recent study on the effect of CheW also provides indirect support for the central role of the trimer of dimers (Cardozo et al. 2010). In evolutionary terms, the structure of the trimer of dimers and the underlying signaling mechanism is highly preserved and could be a universal architecture for many bacterial species (Briegel et al. 2009). Therefore, it is appropriate to thoroughly understand the dynamics of this basic functional unit before postulating models for the effects of higher-order organization.

Our objective here is to develop a complete dynamic model for a single trimer of dimers. Three recent models (Rao et al. 2004a; Endres et al. 2007; Park et al. 2007) of the network focus on the steady-state or equilibrium behavior and treat the upstream steps of ligand binding and kinase activity regulation. In contrast, we treat the ternary complex of a trimer of receptor dimers, a CheA dimer and two CheW monomers as a signaling unit, we incorporate the sensing scheme into the downstream phosphorylation cascade and methylation chain, and we simulate the dynamic behavior of the overall pathway for different types of stimuli. We also perform detailed sensitivity analysis, robustness analysis and system reduction for the model to arrive at a more mechanistic understanding of the structure-function relationships in the signaling system. For example, we test the response to variations in the ligand affinity as a function of the activity of receptors, their methylation level, and the number of ligands bound to receptors, the factors for which different assumptions are made in existing models. Furthermore, we do not use data fitting to establish model parameters; rather, we base the parameter set on the available experimental measures or estimates. In essence, the model we develop is an updated version of an earlier model (Spiro et al. 1997), modified to incorporate new findings on the structure of the receptor complex.

2 Model Development

The signal transduction pathway in *E. coli* chemotaxis can be divided into three steps, ligand binding and kinase activity regulation that occurs on a time scale of milliseconds, phosphoryl transfer on intermediate time scales from tenth of seconds to seconds, and methylation/demethylation on time scales ranging from seconds to minutes, depending on the size of the stimulus. The input to the signaling module is the concentration of ligands, and the output is the concentration of the response regulator protein $CheY_p$. Figure 1 illustrates the states of the signaling complex and the network of transitions among them. The signaling complex, which we denote by T, consists of a trimer of identical receptor dimers (which we call pure-type; mixed-type trimers will be discussed later), a CheA dimer and two CheW monomers, the stoichiometry of which is estimated from several experimental studies (Liu et al. 1997; Francis et al. 2002, 2004; Levit et al. 2002). Receptor trimers and CheA/CheW proteins are assumed to form static signaling complexes in that the estimated half-life of receptor trimers is much longer than the time scales of the reactions that receptors and CheA are involved in Liberman et al. (2004).

Each signaling complex is characterized by its ligand occupancy, the state of its CheA and its methylation level. Throughout we assume that at most one ligand binds to a receptor dimer, since the binding affinity of the second aspartate to a Tar dimer is at least 450-fold lower than that of the first (Bjorkman et al. 2001). Thus, there are three equivalent ligand binding sites and therefore, a signaling complex has four ligand binding states *0*, *1*, *2*, and *3* denoted by the subscript n on T. Concerning the kinase activity of CheA, we assume that a receptor trimer has two conformational states, active and inactive. In the active state, CheA undergoes autophosphorylation and phosphotransfer, whereas in the inactive state the trimer inhibits the autophosphorylation activity of CheA. We assume that both monomers in dimeric CheA phosphorylate or dephosphorylate simultaneously, which means that a signaling complex has three activity states, inactive, active-unphosphorylated and active-phosphorylated, denoted by the superscript $s = i$, a or p on T. Concerning methylation, we focus primarily on the chemotactic response to aspartate. The aspartate receptor Tar has four methylation sites and the wild-type responses probably involve only increases in the average methylation level above the unstimulated level of about 1.5–2 methyl esters per receptor monomer (methylation level 1.5–2) (Boyd and Simon 1980). Therefore, we assume that a trimer with 6 monomers can be methylated to the maximum level of 12, and thus a signaling complex has thirteen methylation states, denoted by the subscript $m = 0, 1, \ldots, 12$ on T.

Changes in the trimer state are encoded in the transition network (Fig. 1). Vertical transitions represent ligand binding (downward) and release (upward). Front-to-rear and reverse transitions involve kinase activity change and phosphoryl transfer. The first step is activation and deactivation of CheA by the trimer, and the second step involves autophosphorylation of CheA (front to rear) and phosphorylation of CheY and CheB (in reverse). Upon removal of the phosphoryl group from CheA, the signaling complex is assumed to return to the active state, i.e., there is no direct transition between the phosphorylated and the inactive state. $CheB_p$ and $CheY_p$ autodephosphorylate and CheZ enhances dephosphorylation of $CheY_p$. Horizontal transitions involve
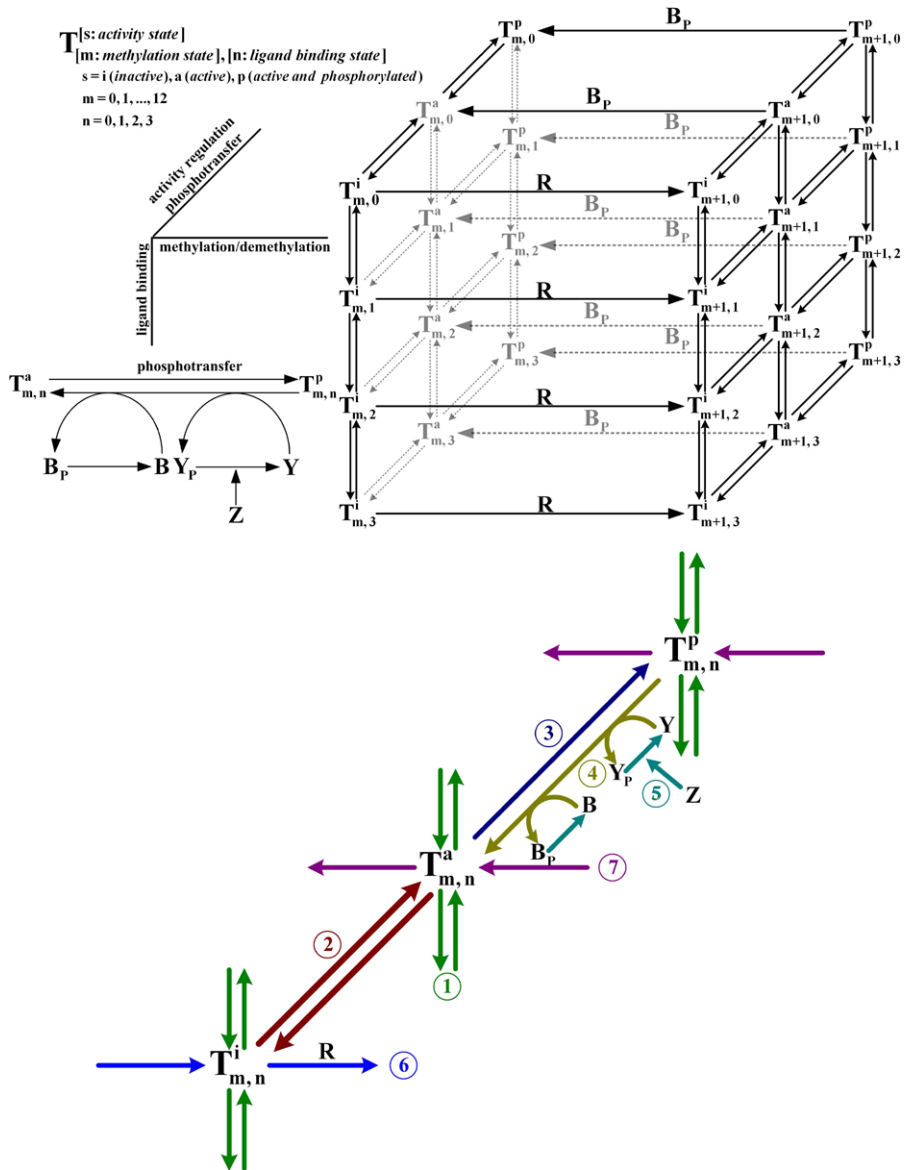
Fig. 1 Signal transduction network. The basic unit of the network is the signaling complex, denoted by T. The three indices used to denote the properties of the complex are shown in the upper left corner. In the reaction network, vertical transitions are ligand binding and release, horizontal transitions are methylation and demethylation, and front-to-rear and reverse transitions are kinase activation, deactivation, phosphorylation, and dephosphorylation. The details of the phosphotransfer transitions are depicted at the *left*. A typical transition chain in the network is expanded in the *lower part* of the figure, where the reactions of the same type are marked with the *same color* and labeled with the *same number*. See also Table 1 (Color figure online)

Table 1 Kinetics and rates of the reactions depicted in Fig. 1

Label and description	Kinetics	Rate	Value	Reference
① ligand binding	$T_{m,n}^a + L \underset{(n+1)k_{-(n+1)}^m}{\overset{(3-n)k_{n+1}^m}{\rightleftharpoons}} T_{m,n+1}^a$	k_n^m k_{-n}^m	Tables 3 & 5 Tables 3 & 5	Bornhorst and Falke (2001, 2003), Li and Weis (2000) Bornhorst and Falke (2001, 2003), Li and Weis (2000)[a]
② activity regulation	$T_{m,n}^a \underset{k_{-i}^{m,n}}{\overset{k_i^{m,n}}{\rightleftharpoons}} T_{m,n}^i$	$K_i = \frac{k_i^{m,n}}{k_{-i}^{m,n}}$ [b]	Tables 3 & 5	Bornhorst and Falke (2001, 2003)[c]
③ autophosphorylation	$T_{m,n}^a \overset{k_A}{\rightarrow} T_{m,n}^p$	k_A	100 s^{-1}	Sourjik and Berg (2002b), Francis et al. (2002)
④ phosphotransfer	$T_{m,n}^p + Y \underset{K_Y}{\rightleftharpoons} [T_{m,n}^p Y] \overset{k_{Y_1}}{\rightarrow} T_{m,n}^a + Y_p$	k_{Y_1} K_Y	200 s^{-1} 0.65 μM^{-1}	Sourjik and Berg (2002b), Stewart et al. (2000), Li et al. (1995) Li et al. (1995)
	$T_{m,n}^p + B \underset{K_B}{\rightleftharpoons} [T_{m,n}^p B] \overset{k_{B_1}}{\rightarrow} T_{m,n}^a + B_p$	k_{B_1} K_B	30 s^{-1} 0.25 μM^{-1}	Stewart et al. (2000), Li et al. (1995) Li et al. (1995)
⑤ dephosphorylation	$Y_p + Z \underset{K_Z}{\rightleftharpoons} [Y_p Z] \overset{k_Z}{\rightarrow} Y + Z$	k_Z K_Z	10 s^{-1} 1 μM^{-1}	Sourjik and Berg (2002b), Kollmann et al. (2005), Silversmith et al. (2001) Sourjik and Berg (2002b), Silversmith et al. (2001)[d]
	$Y_p \overset{k_{Y_2}}{\rightarrow} Y$	k_{Y_2}	0.1 s^{-1}	Sourjik and Berg (2002b)
⑥ methylation	$B_p \overset{k_{B_2}}{\rightarrow} B$	k_{B_2}	1 s^{-1}	Kollmann et al. (2005), Rao et al. (2004b)
	$T_{m,n}^i + R \underset{K_R}{\rightleftharpoons} [T_{m,n}^i R] \overset{k_{R_1}}{\rightarrow} T_{m+1,n}^i + R$	k_{R_1} K_R	0.255 s^{-1} 0.15 μM^{-1}	Morton-Firth et al. (1999), Rao et al. (2004b) Morton-Firth et al. (1999), Barkai and Leibler (1997)[d]
⑦ demethylation	$T_{m,n}^a + B_p \underset{K_{B_p}}{\rightleftharpoons} [T_{m,n}^a B_p] \overset{k_{B_3}}{\rightarrow} T_{m-1,n}^a + B_p$	k_{B_3}	0.5 s^{-1}	Morton-Firth et al. (1999), Rao et al. (2004b)
	$T_{m,n}^p + B_p \underset{K_{B_p}}{\rightleftharpoons} [T_{m,n}^p B_p] \overset{k_{B_3}}{\rightarrow} T_{m-1,n}^p + B_p$	K_{B_p}	6.5 μM^{-1}	Morton-Firth et al. (1999), Barkai and Leibler (1997)[d]

[a] The cooperativity coefficients in ligand affinity are estimated here

[b] For simplicity, we define $p_{m,n}$ as the probability of the unphosphorylated signaling complex with n ligands bound and m methyl groups being in the active state, and then $p_{m,n} = \frac{1}{1+K_i}$. Estimate of $p_{m,n}$ is reported in Tables 3 & 5

[c] The cooperativity coefficients in kinase deactivation are estimated here

[d] The dissociation constant is fine tuned here

methylation (left to right) and demethylation (right to left) of trimers by CheR and CheB$_p$, respectively. We assume that CheR acts only on inactive trimers, and CheB$_p$ only on active ones, either unphosphorylated or phosphorylated. We also assume that the methylation/demethylation rates are the same for ligand-free and ligand-occupied trimers, and that the rates do not depend on the methylation state of trimers.

Since the ligand binding reactions are the fastest, the first component of the response following an increase in attractants is a shift downward to the higher ligand occupancy states. The second component of the response is a redistribution of the activity states from rear to front and a drop in the level of CheY$_p$; this constitutes excitation. The final component of the response involves an increase in the methylation level, hence a shift from left to right, and a corresponding shift in equilibrium between active and inactive states toward the active state. As a result, the lower kinase activity induced by attractant binding on the fast time scale is offset by higher CheA activity in higher-methylation states, and CheY$_p$ returns to the level that prevails in the absence of a stimulus. This constitutes adaptation and completes the response to a step change in attractants.

The mathematical description of the network dynamics is based on mass action kinetics (Table 1) for all steps. For a typical enzyme-catalyzed reaction of the form $E + S \underset{k_1^-}{\overset{k_1^+}{\rightleftharpoons}} [ES] \overset{k_2}{\to} E + P$, the quasisteady-state assumption (QSSA) for the intermediate leads to the rate equation

$$\frac{dP}{dt} = \frac{k_2 E_0 S}{K + S}, \quad \text{where } K = \frac{k_1^- + k_2}{k_1^+},$$

and the conservation condition $E + [ES] = E_0$ for the enzyme has been applied. However, this simple conservation condition does not hold for CheR or CheB$_p$ for an individual methylation or demethylation reaction given by ⑥ or ⑦ in Table 1. Instead, the conservation condition couples all methylation or demethylation reactions. We therefore simplify this by considering the fast time scale of the binding step relative to the following production step, and assume that the kinetics of $[ES]$ can be approximated as $[\dot{ES}] = k_1^+ ES - k_1^- [ES]$. Applying the QSSA to this step yields the modified enzyme kinetic description $\dot{P} = K_a k_2 ES$, where the association constant $K_a = k_1^+ / k_1^-$. The association and disassociation steps between CheY/CheR/CheB/CheB$_p$ and MCP are fast and can be set to equilibrium and therefore, we can apply the above rate law to the bimolecular reactions. Below we only display the equations that govern the evolution of the amounts in the various states of the signaling complexes for $n = 2$; other equations are the same modulo changes in the sub- and superscripts.

$$\frac{dT_{m,2}^i}{dt} = \underbrace{2k_2^m L T_{m,1}^i - 2k_{-2}^m T_{m,2}^i - k_3^m L T_{m,2}^i + 3k_{-3}^m T_{m,3}^i}_{\text{Ligand binding/release}} + \underbrace{k_i^{m,2} T_{m,2}^a - k_{-i}^{m,2} T_{m,2}^i}_{\text{Activity regulation}}$$

$$+ \underbrace{K_R k_{R1} R T_{m-1,2}^i - K_R k_{R1} R T_{m,2}^i}_{\text{Methylation}}, \tag{1}$$

$$\frac{dT_{m,2}^a}{dt} = \underbrace{2k_2^m L T_{m,1}^a - 2k_{-2}^m T_{m,2}^a - k_3^m L T_{m,2}^a + 3k_{-3}^m T_{m,3}^a}_{\text{Ligand binding/release}}$$

$$\underbrace{- k_i^{m,2} T_{m,2}^a + k_{-i}^{m,2} T_{m,2}^i}_{\text{Activity regulation}} - \underbrace{k_A T_{m,2}^a}_{\text{Phosphorylation}}$$

$$\underbrace{+ K_Y k_{Y1} Y T_{m,2}^p + K_B k_{B1} B T_{m,2}^p}_{\text{Phosphotransfer}} \underbrace{- K_{B_p} k_{B3} B_p T_{m,2}^a + K_{B_p} k_{B3} B_p T_{m+1,2}^a}_{\text{Demethylation}},$$

$$(2)$$

$$\frac{dT_{m,2}^p}{dt} = \underbrace{2k_2^m L T_{m,1}^p - 2k_{-2}^m T_{m,2}^p - k_3^m L T_{m,2}^p + 3k_{-3}^m T_{m,3}^p}_{\text{Ligand binding/release}} + \underbrace{k_A T_{m,2}^a}_{\text{Phosphorylation}}$$

$$\underbrace{- K_Y k_{Y1} Y T_{m,2}^p - K_B k_{B1} B T_{m,2}^p}_{\text{Phosphotransfer}} \underbrace{- K_{B_p} k_{B3} B_p T_{m,2}^p + K_{B_p} k_{B3} B_p T_{m+1,2}^p}_{\text{Demethylation}}.$$

$$(3)$$

The equations for CheY$_p$ and CheB$_p$ are

$$\frac{dY_p}{dt} = K_Y k_{Y1} Y \sum_{m=0}^{12} \sum_{n=0}^{3} T_{m,n}^p - k_{Y2} Y_p - K_Z k_Z Z Y_p, \tag{4}$$

$$\frac{dB_p}{dt} = K_B k_{B1} B \sum_{m=0}^{12} \sum_{n=0}^{3} T_{m,n}^p - k_{B2} B_p. \tag{5}$$

In addition, the total amounts of MCP, CheY, CheZ, CheB and CheR are conserved (denoted as T_t, Y_t, Z_t, B_t, and R_t, respectively, in Table 2). For CheY, CheZ, CheB, and CheR, this leads to the equations

$$Y = \frac{Y_t - (1 + K_Z Z) Y_p}{1 + K_Y \sum_{m=0}^{12} \sum_{n=0}^{3} T_{m,n}^p}, \tag{6}$$

$$Z = \frac{Z_t}{1 + K_Z Y_p}, \tag{7}$$

$$B = \frac{B_t - [1 + K_{B_p} \sum_{m=0}^{12} \sum_{n=0}^{3} (T_{m,n}^a + T_{m,n}^p)] B_p}{1 + K_B \sum_{m=0}^{12} \sum_{n=0}^{3} T_{m,n}^p}, \tag{8}$$

$$R = \frac{R_t}{1 + K_R \sum_{m=0}^{12} \sum_{n=0}^{3} T_{m,n}^i}. \tag{9}$$

The four conditions can be used to eliminate four variables, and the resulting system can be integrated numerically upon assignment of parameters. In the following section we define the parameter set.

Table 2 Amounts of chemotactic proteins

Species	Label	Concentration (μM)	Reference
Signaling complex	T_t	5/3[a]	Li and Hazelbauer (2004), Ninfa et al. (1991)
CheR	R_t	0.3	Simms et al. (1987)
CheB	B_t	2	Simms et al. (1985)
CheY	Y_t	18	Alon et al. (1998), Scharf et al. (1998)
CheZ	Z_t	1.1	Sourjik and Berg (2002b)

[a]A signaling complex comprises one trimer of MCP dimers, one CheA dimer and two CheW monomers. In the pure-type model, the MCP is assumed to be Tar. The stoichiometry is Tar:CheA:CheW = 3:1:1. In the mixed-type model, the MCPs are Tar and Tsr, and a receptor trimer consists of one Tar dimer and two Tsr dimers. The stoichiometry is Tar:Tsr:CheA:CheW = 1:2:1:1

3 Parameter Estimation

Parameters such as the ligand binding rates are known experimentally (Bornhorst and Falke 2001, 2003; Li and Weis 2000) but others have to be estimated. A major unknown concerns the activity in the different trimer states. The total kinase activity V_t of the pure-type receptor population is given by $V_t = V_a F_a + V_i F_i$, where F_a (F_i) is the fraction of receptors in the active (inactive) state, and V_a (V_i) is the activity in the active (inactive) state. Here, we assume that $V_i = 0$, i.e., "inactive" receptors are completely inactive, and then $V_t = V_a F_a$. The parameters in activity regulation, $k_i^{m,n}$ and $k_{-i}^{m,n}$ in Table 1, vary with the methylation level because covalent adaptation alters the distribution of receptors in activity states (Starrett and Falke 2005). Concerning other microscopic parameters such as the ligand dissociation constant of inactive (active) receptors K_D^i (K_D^a) and the individual activity V_a, Bornhorst and Falke have shown that a homogeneous two-state model (the methylation level has no effect on other microscopic parameters of the active and inactive states) fails to account for the observed linear correlation of the apparent attractant affinity ($K_{1/2}$) and the kinase activity in the absence of ligands (V^0) (Bornhorst and Falke 2003). They tested six heterogeneous models in which one of (1) K_D^i, (2) K_D^a, (3) V_a, (4) V_i, (5) cooperative interaction between trimers and (6) stability of signaling complexes can vary with the methylation level, and found that the modified model using a variable K_D^i can reproduce the linear correlation (Bornhorst and Falke 2003). Their findings do not rule out the simultaneous change of any combination of the six parameters, and we assume that both K_D^i and K_D^a can be altered.

Next, we set up the rate constants in activity regulation, $k_i^{m,n}$ and $k_{-i}^{m,n}$. There are no available experimental measures for them, but they can be estimated from the observed kinase activity of the reconstituted signaling complexes in the absence of attractants (Table 1 in Bornhorst and Falke 2003). Let $K_i = k_i^{m,n}/k_{-i}^{m,n}$ denote the deactivation equilibrium constant, and define $p_{m,n}$ as the probability that an unphosphorylated signaling complex with n ligands bound and m methyl groups is in the active state. The two are related by $p_{m,n} = 1/(1 + K_i)$. We start from the ligand-free case. In the absence of ligands, the linear relation $V_t = V_a F_a$ is labeled as $V_t^0 = V_a^0 F_a^0$. If we apply the QSSA to the ligand-free activity regulation, we have

$p_{m,0} \approx F_a^0 = V_t^0/V_a^0$. V_a^0, the maximal activity in the absence of ligands, has been estimated. Assuming that the fully methylated state QQQQ drives a receptor population completely into the active state, then $V_a^0 = 3.5$; alternatively, assuming that one of the most active mutants, G278V in the QQQQ state, traps the population fully in the active state, which prevents both attractant-triggered inhibition of kinase activity and demethylation-induced loss of activity, then $V_a^0 = 5.5$ (Bornhorst and Falke 2003). We use the former value to convert the kinase activity to the fraction of active signaling complexes. Since aspartate and α-methyl-aspartate inhibit the kinase activity of Tar, it is expected that $p_{m,n}$ decreases with n. In addition, $p_{m,2}$ and $p_{m,3}$ may be significantly less than $p_{m,0}$ and $p_{m,1}$, even approaching zero, because the observed kinase activity approaches zero under a saturating stimulus (Bornhorst and Falke 2003). Thus, we assume that $p_{m,1}$, $p_{m,2}$, and $p_{m,3}$ are 2, 10, and 100 times less than $p_{m,0}$, respectively, and this leads to the ratios of rate constants given in Table 3. For the individual rates, we can either impose thermodynamic constraints to determine specific rates or apply the QSSA to the activity regulation steps, for which only the relative ratios are necessary because the transition is in essence a conformational change in the cytoplasmic domain of a receptor and it is much faster than other reactions, which involve two proteins. We have tested both methods, and for our choice of the transition rates the QSSA is an excellent approximation, and we use it hereafter. This leads to the following reduced system for the evolution of the receptor states. Hereafter, $T_{m,n}$ denotes the combined active and inactive states of a complex.

$$\frac{dT_{m,2}}{dt} = 2k_2^m L T_{m,1} - 2k_{-2}^m T_{m,2} - k_3^m L T_{m,2} + 3k_{-3}^m T_{m,3} - k_A p_{m,2} T_{m,2}$$

$$+ K_Y k_{Y1} Y T_{m,2}^p + K_B k_{B1} B T_{m,2}^p + K_R k_{R1} R \big[(1 - p_{m-1,2}) T_{m-1,2}$$

$$- (1 - p_{m,2}) T_{m,2}\big] + K_{B_p} k_{B3} B_p (p_{m+1,2} T_{m+1,2} - p_{m,2} T_{m,2}), \quad (10)$$

$$\frac{dT_{m,2}^p}{dt} = 2k_2^m L T_{m,1}^p - 2k_{-2}^m T_{m,2}^p - k_3^m L T_{m,2}^p + 3k_{-3}^m T_{m,3}^p + k_A p_{m,2} T_{m,2}$$

$$- K_Y k_{Y1} Y T_{m,2}^p - K_B k_{B1} B T_{m,2}^p - K_{B_p} k_{B3} B_p \big(T_{m,2}^p - T_{m+1,2}^p\big). \quad (11)$$

Thirdly, we set up the rate constants for ligand binding and release. We begin with a receptor dimer. The rates of aspartate binding to and release from a Tar dimer are 70 µM^{-1} s^{-1} and 70 s^{-1}, respectively (Stock 1994; Spiro et al. 1997). We use α-methyl-aspartate as the attractant in the simulations, and the α-methyl-aspartate affinity of Tar is about 10 times less than aspartate (Albert et al. 2004). Therefore, we assume that the ligand release rate of a dimer is 10 times larger than the aspartate release rate, whereas the ligand binding rate is the same as the aspartate binding rate. In the absence of experimental evidence to the contrary, we assume that receptors have the same ligand affinity in the active and inactive states. Since a heterogeneous two-state assumption is adopted, the ligand dissociation constant depends on the methylation level, and we use the factors $K_D^i = 8.4$ µM, 19 µM, 44 µM, and 67 µM for

Table 3 Rates of ligand binding and kinase activity regulation in pure-type simulation

Rate	Methylation level				
	0–1	2–4	5–7	8–10	11–12
k_1^m ($\mu M^{-1} s^{-1}$)	70	70	70	70	70
k_2^m ($\mu M^{-1} s^{-1}$)	70	70	70	70	70
k_3^m ($\mu M^{-1} s^{-1}$)	70	70	70	70	70
k_{-1}^m (s^{-1})	$700*3.6$	$700*8.4$	$700*19$	$700*49$	$700*67$
k_{-2}^m (s^{-1})	$700*3.6/5$	$700*8.4/5$	$700*19/5$	$700*49/5$	$700*67/5$
k_{-3}^m (s^{-1})	$700*3.6/50$	$700*8.4/50$	$700*19/50$	$700*49/50$	$700*67/50$
$p_{m,0}$	0	0.10	0.29	0.51	0.89
$p_{m,1}$	0	$0.10/2$	$0.29/2$	$0.51/2$	$0.89/2$
$p_{m,2}$	0	$0.10/10$	$0.29/10$	$0.51/10$	$0.89/10$
$p_{m,3}$	0	$0.10/100$	$0.29/100$	$0.51/100$	$0.89/100$

receptors in the methylation state QEEE, QEQE, QQEQ, and QQQQ, respectively, as estimated in Bornhorst and Falke (2003). In addition, $K_D^i = 3.6$ μM for EEEE is interpolated from the above data, and the corresponding ligand release rates are scaled. A remaining question is whether the ligand affinity varies when multiple ligands bind to a trimer. We assume that positive cooperativity exists in the ligand binding sequence and that the affinities of the singly- and doubly-bound trimers, either active or inactive, are 5 and 50 times larger than that of the ligand-free trimers, respectively. This fixes the ligand binding and release rates for the five methylation states EEEE, QEEE, QEQE, QQEQ, and QQQQ. We next assume that the rates only depend on the methylation level (the combination of Q and E), not on the methylation state (a permutation of Q and E), and thereby we obtain a complete set of rates for a dimer. As the last step, we map the rates from a dimer to a trimer of dimers. The accurate mapping is complicated, if not impossible, because it concerns the stochastic nature of the process, such as which dimer member of the trimer a ligand binds to, whether CheR and CheB$_p$ modify methylation sites in sequence of dimer members, in parallel among dimer members of the trimer, or in another order. Here, we do a simple linear mapping: we dissect the full range of the methylation level of a trimer to five sections and map each to one level of a dimer in order. This enables us to assign the ligand binding and release rates k_n^m and k_{-n}^m as in Table 3. The two assumptions we have made here, namely, independence of ligand dissociation constants with receptor activity, and positive cooperativity when multiple ligands bind to a trimer, are discussed in Sect. 7.

Lastly, the rates in phosphorylation, phosphoryl transfer, methylation and demethylation are well documented in literature, but vary due to the different experiment settings. We base ours on the most widely-used values with only minor changes (cf. Table 1 for details). In the following section, we display the computational results for several experimental settings.

4 Results

4.1 Activity Variation with the Methylation Level

In the first set of computations, we remove the methylation and demethylation terms in (10) and (11)[2] to simulate the *in vitro* experiments reported in Bornhorst and Falke (2001, 2003), wherein the kinase activity as a function of ligand concentration was studied for five fixed methylation levels. We compute the fraction of active (both unphosphorylated and phosphorylated) receptors and scale it to the relative kinase activity using the linear relationship $V_t = V_a F_a$, where $V_a = 3.5$ (Bornhorst and Falke 2003). The results of the computation are shown in Fig. 2(A) as open symbols. To further compare the simulated and experimental results, we fit the computed activities with the Hill function

$$V_t = V_t^0 \left(1 - \frac{L^H}{L^H + K_{1/2}^H} \right). \tag{12}$$

The parametric values of (12) in data fitting are compared with the experimental estimates, given in Table 4.

The curves in Fig. 2A capture the observed decay of kinase activity at saturating ligand concentrations. As expected, the apparent dissociation constant of α-methyl-aspartate increases dramatically with the methylation level, whereas the Hill coefficients vary little. A linear correlation between the apparent dissociation constant and the maximal relative activity, as observed in experiments (Bornhorst and Falke 2003), is reproduced in Fig. 2B. The prediction is in good qualitative agreement with the studies (Bornhorst and Falke 2001, 2003; Li and Weis 2000; Levit and Stock 2002) and in quantitative agreement with the experiments we modeled for Bornhorst and Falke (2001, 2003).

To further validate the framework and the parameter set, we simulate another *in vitro* study in which L-aspartate was used, and the apparent dissociation constant of L-aspartate for receptors fixed in the QEQE state estimated as 7.5 ± 1.7 μM (Borkovich et al. 1992). We remove the 10-fold factor in the ligand release rate for a dimer, which is specifically assumed for α-methyl-aspartate in the simulation. The resulting apparent dissociation constant for QEQE is $K_{1/2} = 2.01$ μM, which is three-fold lower than the reported value, but the difference may result from the different strains used in the two experiments.

Table 4 Parameters for fitting the simulation results in Fig. 2 (*top row*) and comparison to the experimental measures in Bornhorst and Falke (2001, 2003) (*bottom row*)

V_t^0				$K_{1/2}$ (μM)				H			
QQQQ	QQQE	QEQE	QEEE	QQQQ	QQQE	QEQE	QEEE	QQQQ	QQQE	QEQE	QEEE
3.16	1.85	1.06	0.36	96.79	69.45	26.53	11.91	2.10	2.06	2.05	2.06
3.1 ± 0.4	1.4 ± 0.1	1.0 ± 0.1	0.36 ± 0.06	97 ± 4	54 ± 6	23 ± 4	9 ± 1	2.2 ± 0.2	2.0 ± 0.5	1.8 ± 0.1	1.7 ± 0.1

---

[2]Of course, we do this for the analogous equations for other (m,n) as well, but we will not repeat this qualifier hereafter.
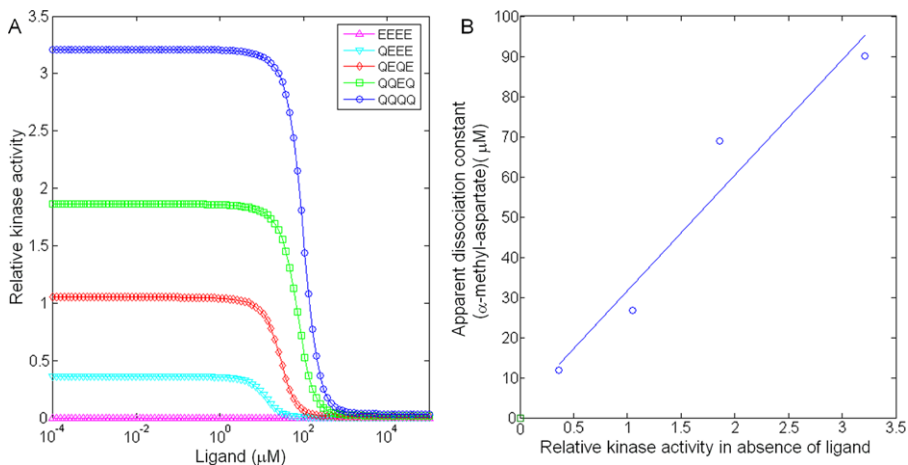
Fig. 2 (**A**) Relative kinase activity of signaling complexes as a function of α-methyl-aspartate concentration for five fixed methylation levels, compared to Fig. 2(c) in Bornhorst and Falke (2001) and Fig. 3(b) in Bornhorst and Falke (2003). (**B**) Correlation of apparent dissociation constant $K_{1/2}$ (α-methyl-aspartate) and relative kinase activity in the absence of ligand V_t^0, compared to Fig. 4 in Bornhorst and Falke (2003) (Color figure online)

4.2 Excitation and Adaptation

To determine whether the model can reproduce the excitation and adaptation behavior, we simulate the system (10) and (11) with the evolution equations (4) and (5). The time courses of CheY$_p$ in response to small and large stimuli are shown in Fig. 3. We also remove the proteins CheR and CheB from the system and simulate the responses of the *cheRcheB* mutant. Both can be compared to the observation with FRET imaging (Fig. 1 in Sourjik and Berg 2002a). Clearly, the time spent to adapt to addition of α-methyl-aspartate varies with the dose of the input. The time to adapt to removal of α-methyl-aspartate seemingly does not change much with the dose. As shown in Fig. 3A4, the adaptation time following addition of a large dose of α-methyl-aspartate is longer than that for removal, which is in agreement with the experimental results (see the *wt* curve in Fig. 1B of Sourjik and Berg 2002a). It indicates that demethylation is more rapid than methylation, which reflects the relative amounts of CheB and CheR. We show later that an increase in the amount of CheR reduces the adaption time following addition of attractants, as expected.

4.3 Sensitivity Analysis

To isolate the primary source of high sensitivity, we dissect the signaling pathway of the excitation phase into multiple steps and perform sensitivity analysis for each. Using the model for nonadapting cells, we derive analytic formulas for sensitivities of ligand binding, activity regulation, autophosphorylation of CheA and phosphoryl transfer to CheY$_p$. Methylation, demethylation, and phosphoryl transfer to CheB$_p$ are not considered since they are involved in the later adaptation phase. Unlike CheR, CheB has a minor role in the downstream signaling sensitivity in wild-type cells because of its competition for phosphoryl groups with CheY. The reaction causes some
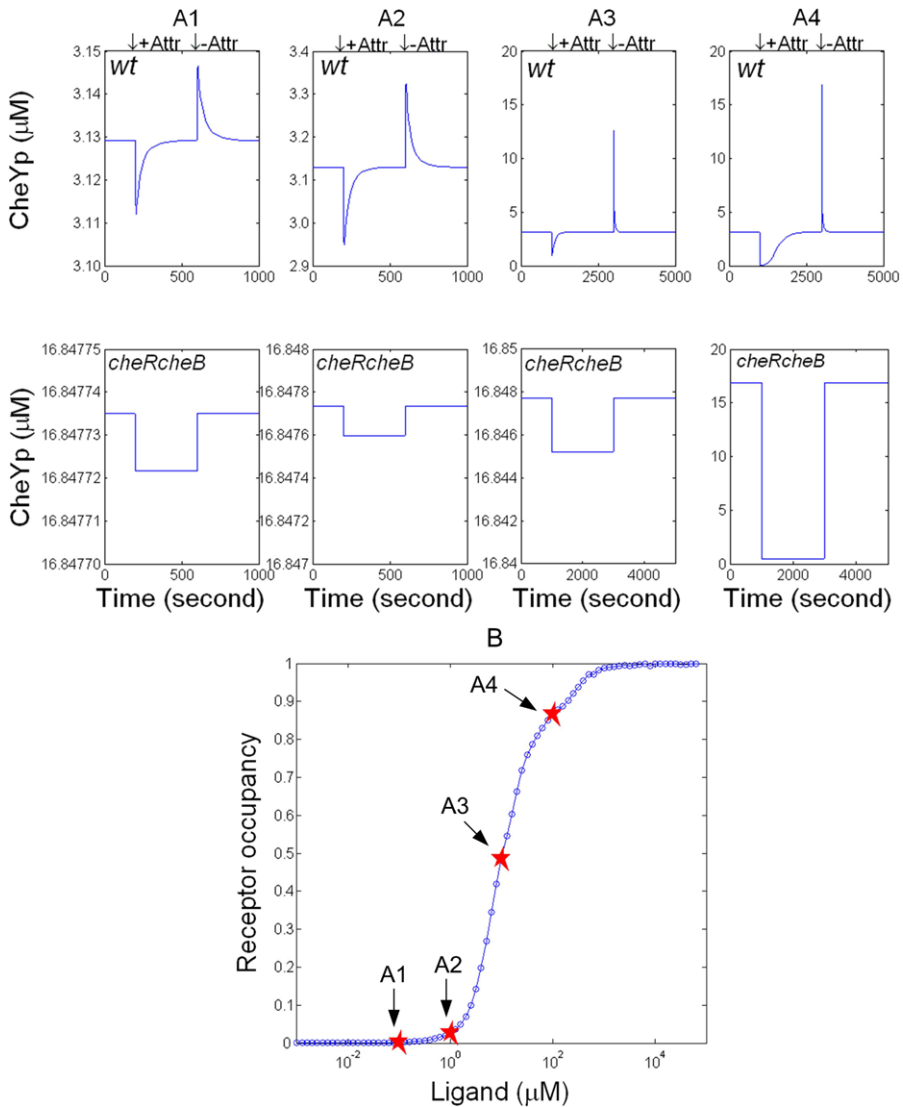
Fig. 3 (**A**) Time course of CheY$_p$ in response to α-methyl-aspartate stimuli predicted by the full system (labeled *wt*) and the nonadapting system (labeled *cheRcheB*). The input is a step of α-methyl-aspartate from 0 μM to 0.1 μM (**A1**), 1 μM (**A2**), 10 μM (**A3**), 100 μM (**A4**), and thereafter a removal of the previous addition. (**B**) Receptor occupancy of α-methyl-aspartate. The *points* corresponding to the ligand concentrations of 0.1 μM, 1 μM, 10 μM, and 100 μM are *highlighted* on the binding curve (Color figure online)

differences in the sensitivity formulas derived for a *cheRcheB* mutant system *vs* a wild-type system. However, inclusion of CheB$_p$ makes it difficult to obtain analytical solutions, and thus we restrict attention to the nonadapting system. The sensitivity profile for each fixed methylation state is similar and therefore, we use the state QEQE as an example.

The sensitivity S of a biochemical pathway is defined as the change of a given state function Y caused by a variation of a given environmental signal X, and can be expressed with an unscaled response function (13) or a scaled dimensionless function (14), if infinitesimal changes are considered (Heinrich et al. 1991). We use the scaled version since it has been widely used in this field (Mello and Tu 2003; Albert et al. 2004; Park et al. 2007).

$$S(Y|X) = \frac{dY}{dX}, \tag{13}$$

$$S(Y|X) = \frac{d\ln Y}{d\ln X}. \tag{14}$$

In the ligand binding step, we define sensitivity as the relative change in ligand occupancy (O) in response to a unit relative change in ligand concentration (L). In the activity regulation step, we define it as the relative change in activity of signaling complexes (A) in response to a unit relative change in ligand occupancy (O). In the phosphorylation step, it is defined as the relative change in amount of the phosphorylated signaling complexes (T^p) in response to a unit relative change in activity of signaling complexes (A). In the phosphoryl transfer step, it is defined as the relative change in amount of CheY$_p$ (Y_p) in response to a unit relative change in amount of the phosphorylated signaling complexes (T^p). Using the definition in (14), we obtain the following results—see the Appendix for the derivation.

$$S(O|L) = \frac{a}{bc}, \tag{15}$$

$$S(A|O) = \frac{cd}{ae}, \tag{16}$$

$$S(T^p|A) = \frac{n_1^2(AT_t)^2 + (2n_1n_3 - n_1n_2)AT_t + n_1AT_t\sqrt{\Delta}}{\Delta + (n_1AT_t - n_2)\sqrt{\Delta}}, \tag{17}$$

$$S(Y_p|T^p) = \frac{k_{Y3}}{k_{Y1}T^p + k_{Y3}}. \tag{18}$$

L : ligand concentration,

O : fraction of the occupied binding sites, defined as

$$O = \frac{\sum_{n=0}^3 (nT_n)}{3T_t},$$

A : fraction of the active signaling complexes, defined as

$$A = \frac{\sum_{n=0}^3 (T_n^a + T_n^p)}{T_t} = \frac{\sum_{n=0}^3 (p_nT_n)}{T_t},$$

where p_n is the probability of the signaling complex with n ligands bound being active,

T^p : concentration of the phosphorylated signaling complex,

Y_p : concentration of the phosphorylated CheY$_p$,

$$a = 1 + \frac{4L}{K_{d2}} + \frac{3L^2}{K_{d1}K_{d2}} + \frac{3L^2}{K_{d2}K_{d3}} + \frac{4L^3}{K_{d1}K_{d2}K_{d3}} + \frac{L^4}{K_{d1}K_{d2}^2K_{d3}},$$

$$b = 1 + \frac{3L}{K_{d1}} + \frac{3L^2}{K_{d1}K_{d2}} + \frac{L^3}{K_{d1}K_{d2}K_{d3}},$$

$$c = 1 + \frac{2L}{K_{d2}} + \frac{L^2}{K_{d2}K_{d3}},$$

$$d = (p_1 - p_0)\frac{3L}{K_{d1}} + (p_2 - p_0)\frac{6L^2}{K_{d1}K_{d2}} + (p_2 - p_1)\frac{9L^3}{K_{d1}^2K_{d2}}$$

$$+ (p_3 - p_0)\frac{3L^3}{K_{d1}K_{d2}K_{d3}} + (p_3 - p_1)\frac{6L^4}{K_{d1}^2K_{d2}K_{d3}}$$

$$+ (p_3 - p_2)\frac{3L^5}{K_{d1}^2K_{d2}^2K_{d3}},$$

$$e = p_0 + p_1\frac{3L}{K_{d1}} + p_2\frac{3L^2}{K_{d1}K_{d2}} + p_3\frac{L^3}{K_{d1}K_{d2}K_{d3}},$$

$$k_{Y3} = k_{Y2} + k_Z Z,$$

$$n_1 = k_A k_{Y1},$$

$$n_2 = k_A k_{Y3} + k_{Y1} k_{Y3} Y_T,$$

$$n_3 = k_A k_{Y3},$$

$$\Delta = n_1^2 (AT_t)^2 + (4n_1 n_3 - 2n_1 n_2)AT_t + n_2^2.$$

Obviously, the sensitivities are multiplicative because if $Z = f(Y) = f(g(X))$, then $S(Z|X) = d\ln Z/d\ln X = d\ln Z/d\ln Y \cdot d\ln Y/d\ln X = S(Z|Y)S(Y|X)$, and thus one can obtain sensitivity for any combination of subsequent steps of the pathway. To demonstrate the contribution of receptor clustering to signaling sensitivity, we also derive the formulas for a hypothetical case in which a signaling complex contains only a receptor dimer (see the Appendix). Figure 4 shows the computational results in both cases. Comparison of Figs. 4A and 4B demonstrates that clustering of dimers into trimers of dimers significantly enhances the overall sensitivity $S(Y_p|L)$, and clearly shows that the enhancement lies in the upstream pathway—namely, in ligand binding and activity regulation. We replot the sensitivities of the two steps in Figs. 4C and 4D, respectively. The enhancement in sensitivity comes from positive cooperativity in ligand binding, which induces the higher ligand affinity of the signaling complexes with more ligands bound, and in activity regulation, which induces a higher degree of activity inhibition (promotion) in the signaling complexes with more attractants (repellents) bound. As a simple test, when we remove the cooperativity assumed in ligand affinities, as expected, the "trimer of dimers" sensitivity reduces to the dotted "dimer" sensitivity curve. It was estimated that in the *cheRcheB* mutant cells with the receptors fixed in the QEQE state, the amplification factor, de-
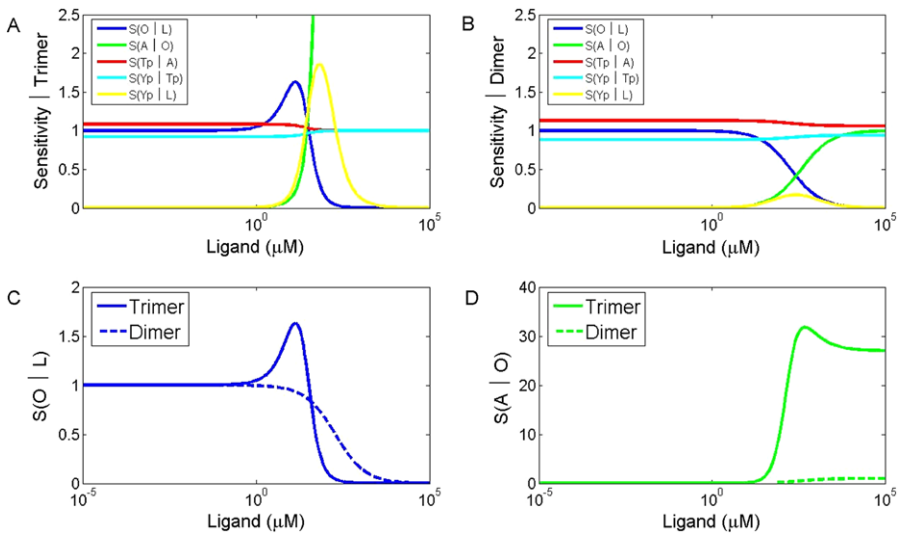
Fig. 4 Sensitivity in signal transduction for two structures of receptor complexes—"trimer of dimers" and "dimer." (**A**) Sensitivities for signaling complexes consisting of "trimer of receptor dimers" in ligand binding $S(O|L)$, activity regulation $S(A|O)$, phosphorylation $S(T^p|A)$, phosphoryl transfer $S(Y_p|T^p)$ and the overall pathway $S(Y_p|L)$. (**B**) Sensitivities for signaling complexes consisting of "receptor dimers" in ligand binding $S(O|L)$, activity regulation $S(A|O)$, phosphorylation $S(T^p|A)$, phosphoryl transfer $S(Y_p|T^p)$ and the overall pathway $S(Y_p|L)$. (**C**) and (**D**) Comparison of $S(O|L)$ and $S(A|O)$ between two structures of receptor complexes (Color figure online)

fined as the fractional change in kinase activity over the fractional change in ligand occupancy, averages 37 ± 9 in response to the fractional changes in attractant concentration of 0.1 or 0.2 (Sourjik and Berg 2002a). In our computation, the sensitivity can be as large as 32 (see the *Trimer* curve in Fig. 4D), which is slightly lower but still close to the measured value.

We also analyze parametric sensitivity in the upstream pathway. Figure 5A shows the sensitivities of receptor occupancy to two parameters—the ligand dissociation constant and the cooperativity coefficient in ligand binding, and Fig. 5B shows the sensitivities of receptor activity to four parameters—the ligand dissociation constant, the probability of a signaling complex being in the active state, and the cooperativity coefficients in ligand binding and activity regulation. An increase of the first ligand dissociation constant reduces receptor occupancy, and the effect declines at saturating ligand concentrations. The changes of receptor occupancy induced by increases of the second and third ligand dissociation constants are similar, and are maximized at intermediate stimuli. An increase of cooperativity in ligand affinity enhances receptor occupancy, and the enhancement is maximized at the moderate stimulus level. Receptor activity increases with the increasing ligand dissociation constants and decreases with the increasing cooperativity coefficients in ligand affinity, and both effects reach a maximum at an intermediate stimulus level. An increase of the probability of a signaling complex being in the active state with any number from 0 to 3 of ligands bound increases receptor activity. At a low stimulus level, the probability p_0 (ligand-free) dominates, and at a high stimulus level the probability p_3 (fully ligand-occupied)
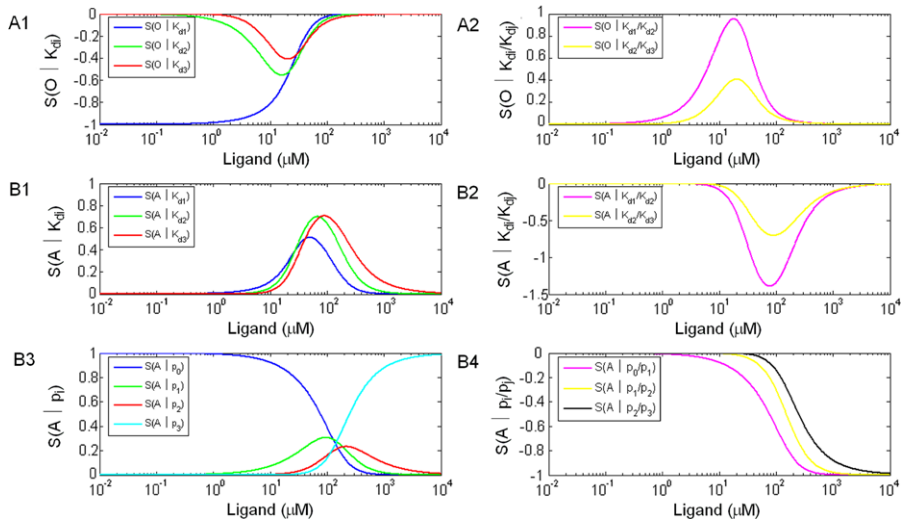
Fig. 5 Parametric sensitivity of receptor occupancy with respect to ligand dissociation constant (**A1**) and to cooperativity in ligand affinity (**A2**); parametric sensitivity of receptor activity with respect to ligand dissociation constant (**B1**), to cooperativity in ligand affinity (**B2**), to the probability of being in the active state (**B3**), and to cooperativity in activity inhibition (**B4**) (Color figure online)

dominates. The probabilities p_1 and p_2 (partially ligand-occupied) function primarily at intermediate stimulus levels. The three cooperativity coefficients in activity regulation have similar effects, that is, an increase of each reduces receptor activity and the reduction saturates at high stimulus levels.

4.4 Robustness Analysis

Next, we investigate the ability of the system to maintain exact adaptation in the face of parametric variations. There is evidence that the *in vivo* signaling network buffers the chemotactic response to variations in the amounts of the chemotactic proteins, including variation in concerted expression of all chemotactic proteins (Kollmann et al. 2005), variation in the expression of CheR (Alon et al. 1999), and variation in the correlated expression of CheY and CheZ (Lřvdok et al. 2007). We employ several simulations to test the robustness of the model to such changes. First, we scale the expression of all receptors and Che-proteins by the same factor and evaluate the effect on adaptation. The variation ranges from 0.1 to 50 fold on a log-linear scale, with the wild-type level treated as fold 1. For each level, we stimulate the cells with a step input of α-methyl-aspartate from 0 μM to 10 μM and record the steady-state post-stimulus values of (i) the adapted concentration of CheY$_p$, (ii) the adaptation time, and (iii) the adaptation precision. The adaptation time is defined as the time at which the concentration of CheY$_p$ in the stimulated cells rises to halfway between the lowest level following stimulation and the steady-state level. The adaptation precision is defined as the ratio between the steady-state concentrations of CheY$_p$ in the prestimulated and adapted cells; a precision of 1 corresponds to prefect adaptation of
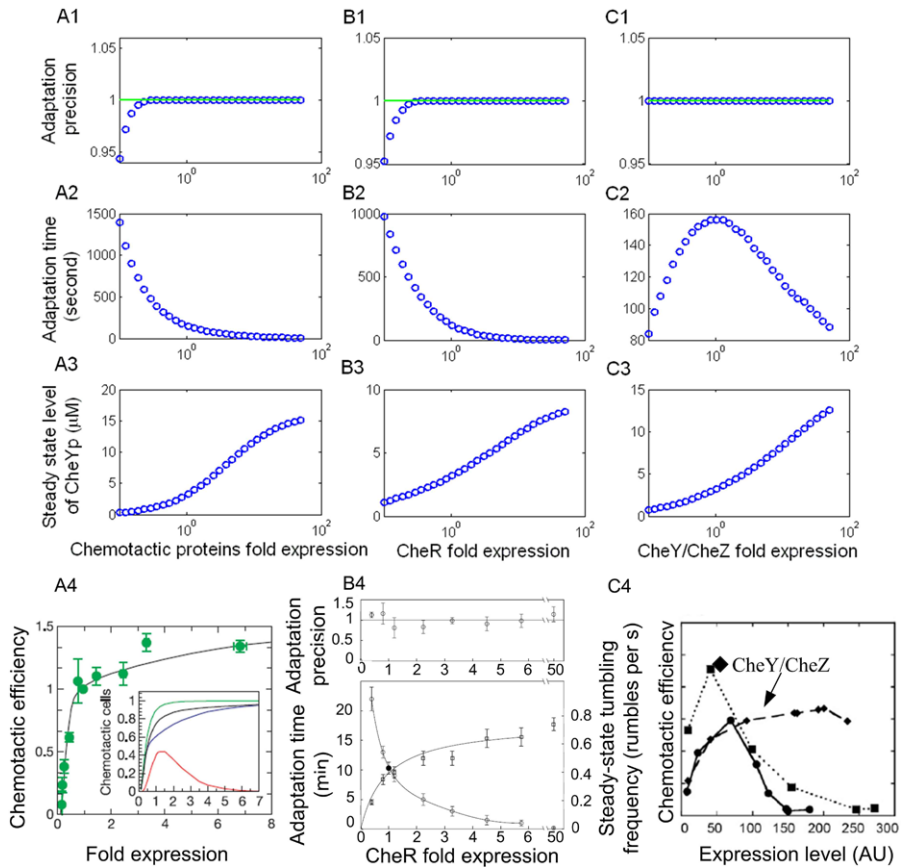
Fig. 6 Robustness of adaptation against variation in concerted expression of all proteins (**A**), expression of CheR (**B**) and correlated expression of CheY/CheZ (**C**). The wild-type concentrations of the proteins are defined as the base level. The stimulus protocol is a step of α-methyl-aspartate from 0 μM to 10 μM. The adaptation precision is robust against the expression levels of all proteins (**A1**), of CheR (**B1**) and of CheY/CheZ (**C1**), while the adaptation time and the steady level of CheY$_p$ are not. The adaptation time decreases with the level of all chemotactic proteins (**A2**) and of CheR (**B2**), and first increases and then decreases with the levels of CheY/CheZ (**C2**). The steady-state level of CheY$_p$ consistently increases with overexpression of all proteins (**A3**), of CheR (**B3**), and of CheY/CheZ (**C3**). The simulations can be compared to the experimental measures of chemotactic efficiency (green circles in **A4**, open circles in the top graph of **B4**, and diamonds in **C4** (from Fig. 1(C) in Lřvdok et al. 2007)), the average adaptation time to a step stimulation with 1mM L-aspartate (open circles in bottom graph of **B4**), and the average steady-state tumbling frequency of the unstimulated cells (open squares in the lower graph of **B4**) (Color figure online)

CheY$_p$. We use the latter definition to facilitate comparison of our results, shown in Fig. 6A, with earlier experimental measures.

One sees that the concerted expression level of all proteins has little effect on exact adaptation of CheY$_p$ (Fig. 6A1), especially in the case of overexpression relative to the wild-type, while the adaptation time decreases significantly (Fig. 6A2) and the adapted steady-state concentration of CheY$_p$ increases significantly (Fig. 6A3). Therefore, the adaptation precision is a robust property of the model, while the adap-
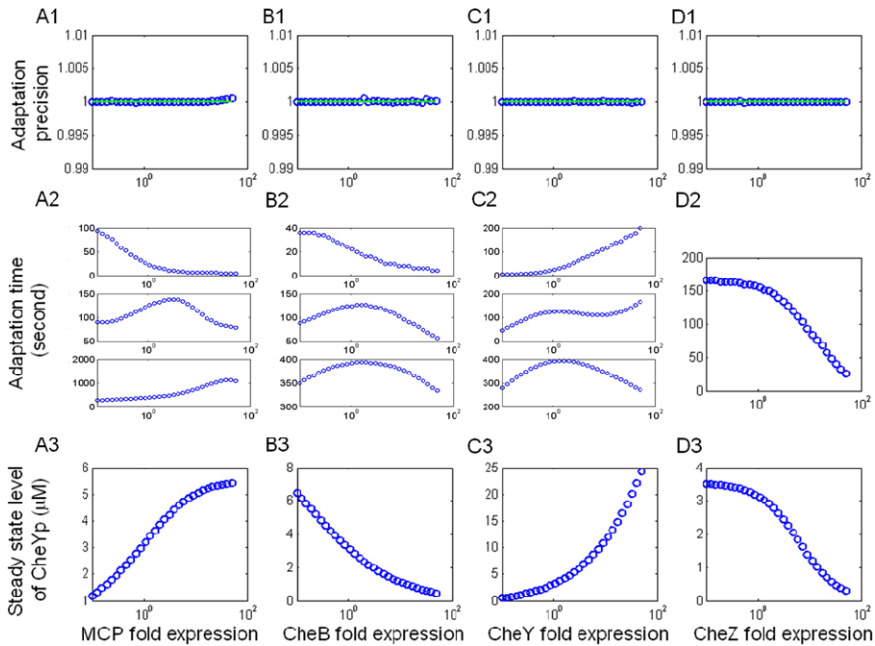
Fig. 7 Robustness of adaptation against variations in expression of chemoreceptor (**A**), CheB (**B**), CheY (**C**), and CheZ (**D**). The definitions of the three displayed variables are as in Fig. 6. The stimulus protocol is a step of α-methyl-aspartate from 0 µM to 10 µM, except in **A2**, **B2**, and **C2**, where three protocols (*top*: 0 µM to 1 µM; *center*: 0 µM to 10 µM; *bottom*: 0 µM to 100 µM) are used to show the change of the adaptation time with the stimulus amplitude (Color figure online)

tation time and the steady-state concentration of $CheY_p$ are not. The increase in $CheY_p$ can be understood from the fact that there are both first- and second-order reactions in the mechanism, and these scale differently under an increase of all components.

The second simulation uses a similar design except that only the level of CheR is varied. One sees again that the adaptation precision is insensitive to the protein level (Fig. 6B1 can be compared to Fig. 2a in Alon et al. (1999), reproduced in Fig. 6A4). The adaptation time and the steady-state level of $CheY_p$ show the decreasing and increasing variation with the CheR expression level similar to those in A2 and A3, respectively. However, comparing Figs. 6A2 and 6B2, one sees that the change of the adaptation time caused by variation of CheR is less than by covariation of all proteins. Figures 6B2 and 6B3 can be compared to 6B4 (Fig. 2b in Alon et al. 1999). The adaptation time we observe differs from that measured in Alon et al. (1999), probably because a step addition of saturating concentrations of attractants was used as the stimulus. One sees in Fig. 3 that the adaptation time increases significantly with the stimulus level.

In the third simulation, we vary the expression levels of CheY and CheZ by the same factor. The effects of the expression levels on the adaptation precision and the steady-state level of $CheY_p$ are similar to the two previous cases, but interestingly, the adaptation time increases with underexpression, reaches maximum at the wild-

type level, and then decreases with overexpression. Increasing only CheY tends to increase the adaptation time, and increasing only CheZ tends to decrease it (Figs. 7C2 and 7D2). Therefore, the former appears to be the dominating effect when CheY and CheZ are coordinately underexpressed and the latter dominates when overexpressed. Lastly, we evaluate the effect on adaptation when the level of chemoreceptors, CheB, CheY, or CheZ is varied individually, and as one sees in Fig. 7, the robustness of adaptation is preserved.

The qualitative variation of the adaptation time in response to addition of attractants that results from under/overexpression of proteins can be understood as follows. Certainly the adaptation time increases with the stimulus amplitude if all other factors are fixed. If the stimulus amplitude is fixed, then the adaptation time varies with the magnitude of the $CheY_p$ response and the available number of CheR/CheB per receptor, and it can be shown that the magnitude of the $CheY_p$ response increases with the steady-state value of $CheY_p$. The effects of other variations are as follows, wherein under/overexpression is relative to the nominal level.

1. *CheR* When the amount of CheR per receptor increases, the adaptation time decreases (Fig. 6B2).
2. *CheZ* An increase in the amount of CheZ decreases the turnover time of $CheY_p$ and reduces the adaptation time (Fig. 7D2).
3. *CheB* An increase in the amount of CheB leads to a monotonic decrease in the steady-state level of $CheY_p$, because the average methylation level of receptors is decreased, which produces a lower kinase activity. However, the change in CheB can have two opposing effects on the adaptation time, as shown in Fig. 7B2, and which dominates can depend on the stimulus level. An increase in CheB leads to a higher level of $CheB_p$ and thus to a lower average methylation level. This in turn shifts the activity equilibrium to the inactive state. Since CheR only acts on inactive receptors, this leads to a higher methylation load and explains the increase in the adaptation time. On the other hand, an increase in CheB reduces the steady-state level of $CheY_p$ (Fig. 7B3) and induces a smaller response of $CheY_p$ and a decrease in the adaptation time. At low stimulus levels, this dominates and the adaptation time is monotone decreasing, but at intermediate and high stimulus levels the larger shift to the inactive state dominates at the low CheB expression levels (Fig. 7B2).
4. *MCP* An increase in MCP also involves two opposing effects, the first of which is an increase in the steady-state level of $CheY_p$ and a larger change in the $CheY_p$ response, which lengthens the adaptation time. The second is a decrease in the ratio of $CheB_p$ to MCP, which reduces the adaptation time (Fig. 7A2) (the steady-state level of $CheB_p$ tends to increase, but the ratio of $CheB_p$ relative to MCP decreases due to the direct overexpression of MCP). In addition, the ratio of CheR to MCP also decreases, which tends to increase the adaptation time, but $CheB_p$ dominates here due to its low abundance compared to CheR.
5. *CheY* An increase in CheY leads to an increase in the $CheY_p$ response and an increase in the adaptation time, but $CheB_p$ decreases and receptors are shifted to higher methylation levels, which decreases adaptation time; which effect dominates depends on the stimulus level and the CheY expression level (Fig. 7C2).

6. *CheY/CheZ* The adaptation time reaches a maximum at the wild-type level, whereas CheY dominates the trend when CheY and CheZ are underexpressed and CheZ dominates when overexpressed (Fig. 6C2).

7. *All proteins* The adaptation time decreases monotonically (Fig. 6A2) because increases in most proteins decrease the adaptation time, which offsets the increase due to the increase in $CheY_p$ (Fig. 6A3).

Changes in the expression levels of MCP, CheB, and CheY all involve two opposing effects on the adaptation time, and the relative roles of the two vary with the stimulus amplitude. The qualitative behavior of the adaptation time can be understood from the roles played by the proteins, but the quantitative aspects represent predictions of the model that may be testable experimentally.

5 Extension to Mixed-Type Model

E. coli has five types of receptors and the different types may interact with each other to achieve an optimal response to diverse environmental stimuli. Experimental evidence shows that receptor trimers may comprise different types of dimers and their assembly involves random recruitment of members from the different dimer pools (Ames et al. 2002; Studdert and Parkinson 2004, 2005). To understand the consequences of receptor heterogeneity, we extend the model for pure receptor types to mixed types, and specifically focus on a combination of Tar and Tsr. Since trimer formation is a stochastic process, a trimer can have one of four compositions, namely three Tar, two Tar one Tsr, one Tar two Tsr, and three Tsr, but the $CheY_p$ response represents an integration over the trimers in all possible compositions. The average *in vivo* ratio of the amounts of Tar and Tsr is 1:2, so the combination of one Tar and two Tsr is the most probable for trimers, and hereafter we neglect the random nature of trimer formation and assume that a trimer comprises one Tar and two Tsr.

In the study of *cheRcheB* mutants, the methylation state of the Tar receptor is fixed at one of EEEE, QEEE, QEQE, and QEQQ, whereas the state of Tsr is fixed at QEQE (Sourjik and Berg 2002a). To simulate the experiments, we adjust the rate assignments in ligand release and kinase activity regulation as shown in Table 5 and Table 6. Here and hereafter, the on rates for ligand binding are as shown in Table 3 and are not repeated. The α-methyl-aspartate affinity of Tsr is roughly one thousand times lower than that of Tar (Albert et al. 2004), and we find that a value of 1500 fits the experimental data well. In light of the large difference, we assume that the ligand binding sequence in a trimer is $TSS \rightarrow T_L SS \rightarrow T_L S_L S \rightarrow T_L S_L S_L$, that is,

Table 5 Ligand release rates in simulations for mixed-type trimers (Tar-Tsr-Tsr)

Rate	Methylation level				
	0–1	2–4	5–7	8–10	11–12
k_{-1}^m (s^{-1})	$700 * 3.6$	$700 * 8.4$	$700 * 19$	$700 * 49$	$700 * 67$
k_{-2}^m (s^{-1})	$700 * 19 * 1500$	$700 * 19 * 1500$	$700 * 19 * 1500$	$700 * 19 * 1500$	$700 * 19 * 1500$
k_{-3}^m (s^{-1})	$700 * 19 * 1500/5$	$700 * 19 * 1500/5$	$700 * 19 * 1500/5$	$700 * 19 * 1500/5$	$700 * 19 * 1500/5$

Table 6 Rates of kinase activity regulation in mixed-type simulations

Rate	Mutant						
	cheR			*cheRcheB*			*cheB*
State of Tar	EEEE	EEEE	QEEE	QEQE	QEQQ	QQQQ	QQQQ
State of Tsr	EEEE	QEQE	QEQE	QEQE	QEQE	QEQE	QQQQ
$p_{m,0}$	0.05	0.61	0.70	0.75	0.84	0.89	0.89
$p_{m,1}$	0.05/3	0.61/3	0.70/1.8	0.75/1.6	0.84/1.4	0.89/1.2	0.89/1
$p_{m,2}$	0.05/9	0.61/9	0.70/5	0.75/2.5	0.84/2	0.89/1.5	0.89/2
$p_{m,3}$	0.05/90	0.61/90	0.70/80	0.75/70	0.84/60	0.89/50	0.89/60

first to the Tar dimer, then to one of the two Tsr dimers, and finally to the remaining unoccupied Tsr dimer. We assign a cooperativity coefficient of 5 in ligand affinity of Tsr to keep the same positive cooperativity assumption as in pure-type, but the factor has little effect here because of the dramatic difference in ligand affinities to Tar and Tsr. The off rates are given in Table 5, where the scaling factor that varies with the methylation level for k^m_{-2} and k^m_{-3} is fixed at 19 since the methylation state of Tsr dimers is fixed at QEQE. The values of the kinase activity parameter $p_{m,n}$ are based on the estimates in Table 3 and the variable factors in activity regulation are adjusted to fit the data. Equations (19) and (20) show one set ($n = 2$, $m =$ fixed methylation level) for the nonadapting system, in which CheR and CheB are deleted.

$$\frac{dT_{m,2}}{dt} = 2k^m_2 L T_{m,1} - k^m_{-2} T_{m,2} - k^m_3 L T_{m,2} + 2k^m_{-3} T_{m,3} - k_A p_{m,2} T_{m,2}$$
$$+ K_Y k_{Y1} Y T^p_{m,2}, \tag{19}$$

$$\frac{dT^p_{m,2}}{dt} = 2k^m_2 L T^p_{m,1} - k^m_{-2} T^p_{m,2} - k^m_3 L T^p_{m,2} + 2k^m_{-3} T^p_{m,3} + k_A p_{m,2} T_{m,2}$$
$$- K_Y k_{Y1} Y T^p_{m,2}. \tag{20}$$

The normalized steady-state concentration of CheY$_p$ predicted for various *cheRcheB* mutants is shown in Fig. 8A and can be compared to Fig. 2 in Sourjik and Berg (2002a) (reproduced as Fig. 6C). The four *cheRcheB* curves have two apparent dissociation constants corresponding to Tar and Tsr and can be fit by a Hill function of the form (Albert et al. 2004)

$$F_{Y_P} = 1 - \beta \frac{L^{H_1}}{L^{H_1} + K_1^{H_1}} - (1 - \beta) \frac{L^{H_2}}{L^{H_2} + K_2^{H_2}}. \tag{21}$$

The values of the Hill coefficient and the half-maximal concentration are reported in Table 7. One sees from Fig. 8 and the table that we obtain both qualitative and quantitative agreement with the reported data in terms of the relative effects of the ligand on the various mutants and the Hill coefficients that fit the various curves. Furthermore, the response amplitudes for the various strains, relative to *cheRcheB*(EEEE) and ordered as *cheR*, *cheRcheB*(EEEE), *cheRcheB*(QEEE),

Table 7 Parameters for fitting the simulations in Fig. 8 and comparison to the experimental measures in (Sourjik and Berg 2002a)

		cheRcheB				*cheR*	*cheB*
		QQQE	QEQE	QEEE	EEEE		
β	Simulation	0.27	0.37	0.44	0.66		
	Experiment	0.27 ± 0.02	0.36 ± 0.02	0.46 ± 0.02	0.65 ± 0.02		
$K_1 (\mu M)$	Simulation	421.41	180.69	84.70	36.14	3.89	
	Experiment	440 ± 70	150 ± 15	80 ± 15	38 ± 5	3.3 ± 0.5	
$K_2 (mM)$	Simulation	105.05	102.21	85.01	83.85		90.0820
	Experiment	110 ± 10	105 ± 19	77 ± 10	83 ± 17		75 ± 18
H_1	Simulation	1.08	1.04	1.00	1.01	2.60	
	Experiment	1.2 ± 0.1					
H_2	Simulation	1.33	1.36	1.40	1.34		1.41
	Experiment	1.2 ± 0.1					

cheRcheB(QEQE), *cheRcheB*(QEQQ), and *cheB*, are 0.05 : 1 : 1.12 : 1.19 : 1.28 : 1.33, respectively, which is to be compared with the experimental observations of 0.04 : 1 : 1.15 : 1.23 : 1.38 : 1.46 for the same sequence. The *cheR* and *cheB* curves have only one apparent dissociation constant, seemingly that of *cheR* corresponding to Tar and that of *cheB* corresponding to Tsr, and both can be fitted using (12).

We also simulate the sensitivity profile for *cheRcheB* mutants, which is defined as the ratio of the relative change in the steady-state level of CheY$_p$ to the relative change in the ligand concentration. We do this by applying a step increase of ambient ligand concentration of $10^{0.08} \mu M$. The result is shown in Fig. 8B and can be compared to the experimental results shown in Fig. 3B in Sourjik and Berg (2002a) (reproduced as Fig. 6D). Our model is able to account for these observations, something that other models have not done to date.

6 Model Reduction

The detailed model is based on the detailed signal transduction network and consists of 158 differential equations, but the input and output relationship of the system is relatively simple, as seen in Figs. 3. This gives rise to the question of whether we can use a simpler model to describe the system. Here, "simpler" means a lower-dimensional system that involves fewer time-varying quantities explicitly. In this section, we apply two different methods to develop simpler systems.

6.1 Model Reduction I: *Multi-Time-Scale Analysis*

In complex reaction networks, fast reactions dominate the initial dynamics and may reach a quasi-steady state quickly, whereas slow reactions dominate the dynamics on a long time scale. The slow dynamics are often of primary interest, and to reduce the number of variables and differential equations with kinetic rates of widely-differing orders of magnitude, techniques have been developed to construct governing equations for slowly-varying quantities that properly account for the fast reactions (Lee
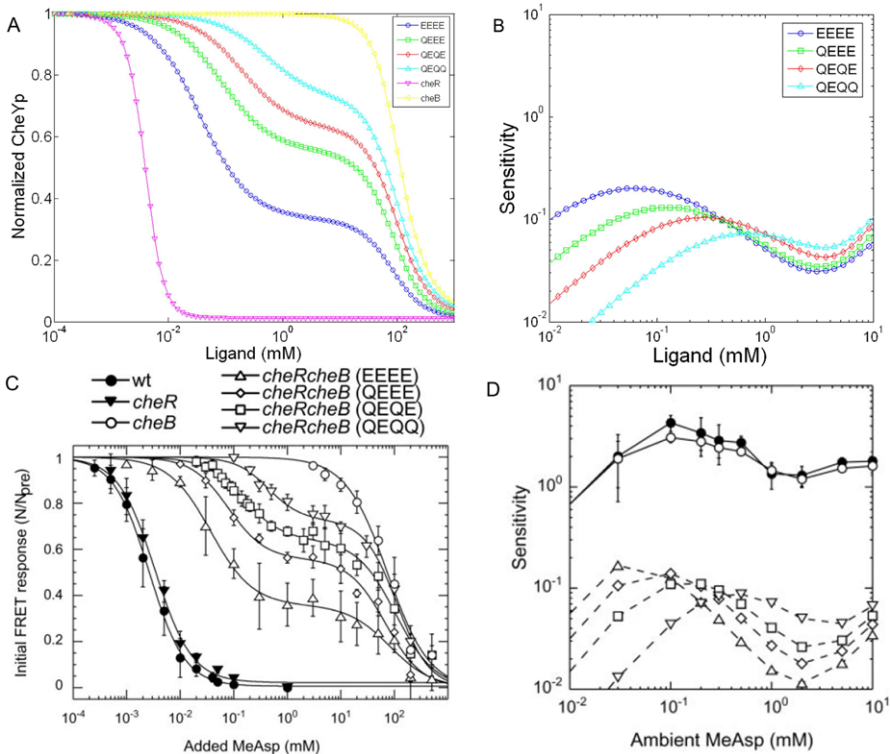
Fig. 8 (**A**) Normalized concentration of CheY$_p$ as a function of ligand concentration. The curves for *cheRcheB* (EEEE), *cheRcheB* (QEEE), *cheRcheB* (QEQE), and *cheRcheB* (QEQQ) are fit with the parameter set in Table 5 in the case of $m = 0$, $m = 3$, $m = 6$, and $m = 9$, respectively. The curve *cheR* is fit with the parameters $k_1^m = k_2^m = k_3^m = 70 \ \mu M^{-1} s^{-1}$, $k_{-1}^m = 700 * 3.6 \ s^{-1}$, $k_{-2}^m = 700 * 3.6 * 0.125 \ s^{-1}$, $k_{-3}^m = 700 * 3.6 * 0.125/10 \ s^{-1}$, $p_{m,0} = 0.05/1.2$, $p_{m,1} = 0.05/1.2/3$, $p_{m,2} = 0.05/1.2/9$, $p_{m,3} = 0.05/1.2/90$. The curve *cheB* is fit with the parameters $k_1^m = k_2^m = k_3^m = 70 \ \mu M^{-1} s^{-1}$, $k_{-1}^m = 700 * 67 \ s^{-1}$, $k_{-2}^m = 700 * 67 * 400 \ s^{-1}$, $k_{-3}^m = 700 * 67 * 400/10 \ s^{-1}$, $p_{m,0} = 0.89 * 1.2$, $p_{m,1} = 0.89 * 1.2$, $p_{m,2} = 0.89 * 1.2/2$, $p_{m,3} = 0.89 * 1.2/60$. (**B**) Sensitivity of the *cheRcheB* mutants in four fixed methylation states to an 8 % log increase in the α-methyl-aspartate concentration. The sensitivity is defined as the ratio of the relative change in the steady-state concentration of CheY$_p$ and the relative change in ligand concentration. The simulations can be compared to the experimentally measured responses of the *cheR* and/or *cheB* cells to steps of MeAsp at 0 ambient (**C** above—Fig. 2 of Sourjik and Berg 2002a) and the sensitivity calculated from the data for the *cheRchB* mutant cells (**D** above—Fig. 3B of Sourjik and Berg 2002a) (Color figure online)

and Othmer 2010). The quasi-steady state assumption (QSSA) approach is one of the classical techniques.

The signal transduction network of *E. coli* chemotaxis includes reactions on three distinct time scales: (1) *fast*, ligand binding and kinase activity regulation reactions in milliseconds, (2) *intermediate*, phosphorylation and phosphoryl transfer reactions in tenth of seconds to seconds, (3) *slow*, methylation and demethylation reactions in seconds to minutes. In Fig. 1, the *fast* and *intermediate* reactions are the transitions in each slice of the network while the *slow* reactions are the transitions between slices.

To derive a reduced system, we apply the QSSA to the fast reactions in series, first to ligand binding and then to activity regulation, while explicitly retaining the dynamics of the intermediate and slow reactions.

Let T_m^n ($m = 0, \ldots, 12$; $n = 0, \ldots, 3$) denote the amount of the signaling complexes with n ligands bound and m methyl groups. Therefore, $T_m^n = T_{m,n}^i + T_{m,n}^a + T_{m,n}^p$. The network of transitions among the pure-type T_m^n is

$$T_m^0 \underset{k_{-1}^m}{\overset{3k_1^m L}{\rightleftharpoons}} T_m^1 \underset{2k_{-2}^m}{\overset{2k_2^m L}{\rightleftharpoons}} T_m^2 \underset{3k_{-3}^m}{\overset{k_3^m L}{\rightleftharpoons}} T_m^3.$$
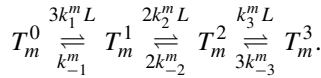
The equations that govern the evolution of the amounts are

$$\frac{dT_m^0}{dt} = -3k_1^m L T_m^0 + k_{-1}^m T_m^1, \tag{22}$$

$$\frac{dT_m^1}{dt} = 3k_1^m L T_m^0 - k_{-1}^m T_m^1 - 2k_2^m L T_m^1 + 2k_{-2}^m T_m^2, \tag{23}$$

$$\frac{dT_m^2}{dt} = 2k_2^m L T_m^1 - 2k_{-2}^m T_m^2 - k_3^m L T_m^2 + 3k_{-3}^m T_m^3, \tag{24}$$

$$\frac{dT_m^3}{dt} = k_3^m L T_m^2 - 3k_{-3}^m T_m^3. \tag{25}$$

Applying the QSSA to the fast reactions, we have

$$q_m^n \equiv \frac{T_m^n}{\sum_{n=0}^3 T_m^n} = \begin{cases} \dfrac{1}{1 + \frac{3L}{K_{d1}^m} + \frac{3L^2}{K_{d1}^m K_{d2}^m} + \frac{L^3}{K_{d1}^m K_{d2}^m K_{d3}^m}} & n = 0 \\[2em] \dfrac{\frac{3L}{K_{d1}^m}}{1 + \frac{3L}{K_{d1}^m} + \frac{3L^2}{K_{d1}^m K_{d2}^m} + \frac{L^3}{K_{d1}^m K_{d2}^m K_{d3}^m}} & n = 1 \\[2em] \dfrac{\frac{3L^2}{K_{d1}^m K_{d2}^m}}{1 + \frac{3L}{K_{d1}^m} + \frac{3L^2}{K_{d1}^m K_{d2}^m} + \frac{L^3}{K_{d1}^m K_{d2}^m K_{d3}^m}} & n = 2 \\[2em] \dfrac{\frac{L^3}{K_{d1}^m K_{d2}^m K_{d3}^m}}{1 + \frac{3L}{K_{d1}^m} + \frac{3L^2}{K_{d1}^m K_{d2}^m} + \frac{L^3}{K_{d1}^m K_{d2}^m K_{d3}^m}} & n = 3. \end{cases} \tag{26}$$

Similarly, for the mixed-type trimers, where a trimer is composed of one Tar homodimer and two Tsr homodimers, we have

$$q_m^n = \begin{cases} \dfrac{1}{1 + \frac{L}{K_{d1}^m} + \frac{2L^2}{K_{d1}^m K_{d2}^m} + \frac{L^3}{K_{d1}^m K_{d2}^m K_{d3}^m}} & n = 0 \\[2em] \dfrac{\frac{L}{K_{d1}^m}}{1 + \frac{L}{K_{d1}^m} + \frac{2L^2}{K_{d1}^m K_{d2}^m} + \frac{L^3}{K_{d1}^m K_{d2}^m K_{d3}^m}} & n = 1 \\[2em] \dfrac{\frac{2L^2}{K_{d1}^m K_{d2}^m}}{1 + \frac{L}{K_{d1}^m} + \frac{2L^2}{K_{d1}^m K_{d2}^m} + \frac{L^3}{K_{d1}^m K_{d2}^m K_{d3}^m}} & n = 2 \\[2em] \dfrac{\frac{L^3}{K_{d1}^m K_{d2}^m K_{d3}^m}}{1 + \frac{L}{K_{d1}^m} + \frac{2L^2}{K_{d1}^m K_{d2}^m} + \frac{L^3}{K_{d1}^m K_{d2}^m K_{d3}^m}} & n = 3. \end{cases} \tag{27}$$

We let T_m ($m = 0, \ldots, 12$) denote the amount of the signaling complexes with the methylation level m, and then $T_m^n = q_m^n T_m$.

We define p_m^n as the probability of a signaling complex with n ligands bound and m methyl groups being active, or equivalently the proportion of the active signaling complexes with n ligands bound and m methyl groups. Thus $T_{m,n}^a + T_{m,n}^p = p_m^n T_m^n$ and $T_{m,n}^i = (1 - p_m^n) T_m^n$. The kinetic step for activity regulation is
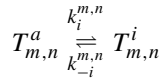
$$T_{m,n}^a \underset{k_{-i}^{m,n}}{\overset{k_i^{m,n}}{\rightleftharpoons}} T_{m,n}^i$$

and applying the QSSA yields $T_{m,n}^i = \frac{K_i}{1+K_i}(T_m^n - T_{m,n}^p)$ and $T_{m,n}^a = \frac{1}{1+K_i}(T_m^n - T_{m,n}^p)$, where $K_i = \frac{k_i^{m,n}}{k_{-i}^{m,n}}$. As an estimate, we have $p_m^n \simeq \frac{1}{1+K_i}$.

T^i, T^a, and T^p are the amounts of the inactive, active-unphosphorylated, and active-phosphorylated signaling complexes, respectively. The equations that govern the evolution of the amounts of T^p, Y_p, and B_p are

$$\frac{dT^p}{dt} = k_A T^a - K_Y k_{Y1} Y T^p - K_B k_{B1} B T^p, \tag{28}$$

$$\frac{dY_p}{dt} = K_Y k_{Y1} Y T^p - k_{Y2} Y_p - K_Z k_Z Z Y_p, \tag{29}$$

$$\frac{dB_p}{dt} = K_B k_{B1} B T^p - k_{B2} B_p. \tag{30}$$

The amount of T^a is determined by the upstream part of the pathway-*ligand binding* and *activity regulation* as follows:

$$T^a = \sum_{m=0}^{12} \sum_{n=0}^{3} (T_{m,n}^a + T_{m,n}^p) - T^p = \sum_{m=0}^{12} \sum_{n=0}^{3} p_m^n T_m^n - T^p = \sum_{m=0}^{12} \sum_{n=0}^{3} p_m^n q_m^n T_m - T^p. \tag{31}$$

The conservation conditions for CheY, CheZ, and CheB are as follows:

$$Y = \frac{Y_t - (1 + K_Z Z) Y_p}{1 + K_Y T^p}, \tag{32}$$

$$Z = \frac{Z_t}{1 + K_Z Y_p}, \tag{33}$$

$$B = \frac{B_t - [1 + K_{B_p}(T^a + T^p)] B_p}{1 + K_B T^p}. \tag{34}$$

The network for the transitions between the T_m (the amount of the signaling complexes with the methylation level m) is

$$\cdots \underset{f_{m-1}^a k^-}{\overset{f_{m-2}^i k^+}{\rightleftharpoons}} T_{m-1} \underset{f_m^a k^-}{\overset{f_{m-1}^i k^+}{\rightleftharpoons}} T_m \underset{f_{m+1}^a k^-}{\overset{f_m^i k^+}{\rightleftharpoons}} T_{m+1} \underset{f_{m+2}^a k^-}{\overset{f_{m+1}^i k^+}{\rightleftharpoons}} \cdots,$$
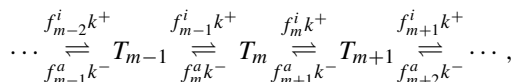
and the equations for the evolution of the amounts are

$$\frac{dT_m}{dt} = (1 - \delta_{m,0})\left(k^+ f_{m-1}^i T_{m-1} - k^- f_m^a T_m\right)$$
$$- (1 - \delta_{m,M})\left(k^+ f_m^i T_m - k^- f_{m+1}^a T_{m+1}\right), \tag{35}$$

where δ is the Kronecker delta.

Next, we derive the four coefficients f_m^i, f_m^a, k^+ and k^- in (35). f_m^i is the proportion of the inactive signaling complexes with m methyl groups and therefore,

$$f_m^i = \frac{\sum_{n=0}^3 T_{m,n}^i}{T_m} = \sum_{n=0}^3 (1 - p_m^n) q_m^n. \tag{36}$$

Similarly, f_m^a is the proportion of the active (phosphorylated and unphosphorylated) signaling complexes with m methyl groups and therefore,

$$f_m^a = \frac{\sum_{n=0}^3 (T_{m,n}^a + T_{m,n}^p)}{T_m} = \sum_{n=0}^3 p_m^n q_m^n. \tag{37}$$

To derive k^+ and k^-, we use mass action kinetics to describe the methylation and demethylation reactions. Consider methylation as an example. A typical transition is

$$T_{m,n}^i + R \underset{k_{R_3}}{\overset{k_{R_2}}{\rightleftharpoons}} \left[T_{m,n}^i R\right] \overset{k_{R_1}}{\rightarrow} T_{m+1,n}^i + R,$$
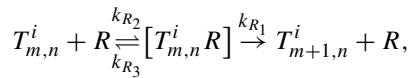
and if we assume that the reversible step equilibrates rapidly, the evolution equation can be written as

$$\frac{dT_{m+1,n}^i}{dt} = K_R k_{R1} R T_{m,n}^i.$$

Therefore,

$$k^+ = K_R k_{R1} R \tag{38}$$

and similarly,

$$k^- = K_{B_p} k_{B3} B_p. \tag{39}$$

Finally, the conservation conditions on CheR and MCP are as follows:

$$R = \frac{R_t}{1 + \left(\frac{k_{R2}}{k_{R3}}\right) \sum_{m=0}^{12} \sum_{n=0}^3 T_{m,n}^i} = \frac{R_t}{1 + K_R T^i}, \tag{40}$$

$$T_t = \sum_{m=0}^{12} T_m. \tag{41}$$

Therefore, the resulting system, which we refer to as I, consists of 16 differential equations: (35) for T_m ($m = 0, \ldots, 12$), (28) for T_p, (29) for Y_p, and (30) for B_p, as summarized below:

$$\frac{dT_m}{dt} = (1 - \delta_{m,0})\big(k^+ f^i_{m-1} T_{m-1} - k^- f^a_m T_m\big)$$
$$- (1 - \delta_{m,M})\big(k^+ f^i_m T_m - k^- f^a_{m+1} T_{m+1}\big),$$

$$\frac{dT^p}{dt} = k_A T^a - K_Y k_{Y1} Y T^p - K_B k_{B1} B T^p,$$

$$\frac{dY_p}{dt} = K_Y k_{Y1} Y T^p - k_{Y2} Y_p - K_Z k_Z Z Y_p,$$

$$\frac{dB_p}{dt} = K_B k_{B1} B T^p - k_{B2} B_p,$$

$$T^a = \sum_{m=0}^{12} \sum_{n=0}^{3} p^n_m q^n_m T_m - T^p,$$

$$Y = \frac{Y_t - (1 + K_Z Z) Y_p}{1 + K_Y T^p},$$

$$Z = \frac{Z_t}{1 + K_Z Y_p},$$

$$B = \frac{B_t - [1 + K_{B_p}(T^a + T^p)] B_p}{1 + K_B T^p},$$

$$R = \frac{R_t}{1 + K_R(T_T - T^a - T^p)},$$

$$T_t = \sum_{m=0}^{12} T_m,$$

$$k^+ = K_R k_{R1} R,$$

$$k^- = K_{B_p} k_{B3} B_p,$$

$$f^i_m = \sum_{n=0}^{3} (1 - p^n_m) q^n_m,$$

$$f^a_m = \sum_{n=0}^{3} p^n_m q^n_m,$$

$$q^n_m = \begin{cases} \dfrac{1}{1 + \frac{3L}{K^m_{d1}} + \frac{3L^2}{K^m_{d1} K^m_{d2}} + \frac{L^3}{K^m_{d1} K^m_{d2} K^m_{d3}}} & n = 0 \\[2em] \dfrac{\frac{3L}{K^m_{d1}}}{1 + \frac{3L}{K^m_{d1}} + \frac{3L^2}{K^m_{d1} K^m_{d2}} + \frac{L^3}{K^m_{d1} K^m_{d2} K^m_{d3}}} & n = 1 \\[2em] \dfrac{\frac{3L^2}{K^m_{d1} K^m_{d2}}}{1 + \frac{3L}{K^m_{d1}} + \frac{3L^2}{K^m_{d1} K^m_{d2}} + \frac{L^3}{K^m_{d1} K^m_{d2} K^m_{d3}}} & n = 2 \\[2em] \dfrac{\frac{L^3}{K^m_{d1} K^m_{d2} K^m_{d3}}}{1 + \frac{3L}{K^m_{d1}} + \frac{3L^2}{K^m_{d1} K^m_{d2}} + \frac{L^3}{K^m_{d1} K^m_{d2} K^m_{d3}}} & n = 3 \end{cases} \quad \text{pure-type},$$

$$q_m^n = \begin{cases} \dfrac{1}{1+\frac{L}{K_{d1}^m}+\frac{2L^2}{K_{d1}^m K_{d2}^m}+\frac{L^3}{K_{d1}^m K_{d2}^m K_{d3}^m}} & n=0 \\[2em] \dfrac{\frac{L}{K_{d1}^m}}{1+\frac{L}{K_{d1}^m}+\frac{2L^2}{K_{d1}^m K_{d2}^m}+\frac{L^3}{K_{d1}^m K_{d2}^m K_{d3}^m}} & n=1 \\[2em] \dfrac{\frac{2L^2}{K_{d1}^m K_{d2}^m}}{1+\frac{L}{K_{d1}^m}+\frac{2L^2}{K_{d1}^m K_{d2}^m}+\frac{L^3}{K_{d1}^m K_{d2}^m K_{d3}^m}} & n=2 \\[2em] \dfrac{\frac{L^3}{K_{d1}^m K_{d2}^m K_{d3}^m}}{1+\frac{L}{K_{d1}^m}+\frac{2L^2}{K_{d1}^m K_{d2}^m}+\frac{L^3}{K_{d1}^m K_{d2}^m K_{d3}^m}} & n=3 \end{cases} \quad \text{mixed-type.}$$

We simulate the time course of $CheY_p$ in response to three varying-dose α-methyl-aspartate stimuli, using both the full system and the reduced system I. The computational results are shown in Fig. 9, and one sees there that the reduced system not only achieves perfect adaptation, but also reproduces the transient and steady-state values of $CheY_p$ in the full system.

6.2 Model Reduction II: *Mean-Field Theory*

A multi-subunit system with interaction among subunits is generally difficult to solve exactly. The great difficulty lies in the treatment of combinatorics generated by the interaction terms in the Hamiltonian when summing over all states, especially when computing the partition function of the system. The mean-field theory, the main idea of which is to replace all interactions to any one subunit with an average interaction, reduces any multi-subunit problem into an effective one-subunit problem. We can consider the clustered, interacting chemoreceptor trimers as such a system and apply the mean-field theory approach to model the methylation states of a trimer of dimers.

Let A_m denote the activity of a signaling complex with the methylation level m, that is, the probability of a signaling complex with the methylation level m being active, which is dependent on the ligand concentration L. The activity A_m is approximated as the proportion of the active signaling complexes with the methylation level m, and the steady-state solution is

$$A_m = \frac{\sum_{n=0}^{3}(T_m^{a,n}+T_m^{p,n})}{T_m} = \sum_{n=0}^{3} p_m^n \frac{T_m^n}{T_m}$$

$$= \begin{cases} \dfrac{p_m^0+p_m^1\frac{3L}{K_{d1}^m}+p_m^2\frac{3L^2}{K_{d1}^m K_{d2}^m}+p_m^3\frac{L^3}{K_{d1}^m K_{d2}^m K_{d3}^m}}{1+\frac{3L}{K_{d1}^m}+\frac{3L^2}{K_{d1}^m K_{d2}^m}+\frac{L^3}{K_{d1}^m K_{d2}^m K_{d3}^m}} & \text{pure-type} \\[2em] \dfrac{p_m^0+p_m^1\frac{L}{K_{d1}^m}+p_m^2\frac{2L^2}{K_{d1}^m K_{d2}^m}+p_m^3\frac{L^3}{K_{d1}^m K_{d2}^m K_{d3}^m}}{1+\frac{L}{K_{d1}^m}+\frac{2L^2}{K_{d1}^m K_{d2}^m}+\frac{L^3}{K_{d1}^m K_{d2}^m K_{d3}^m}} & \text{mixed-type.} \end{cases} \tag{42}$$
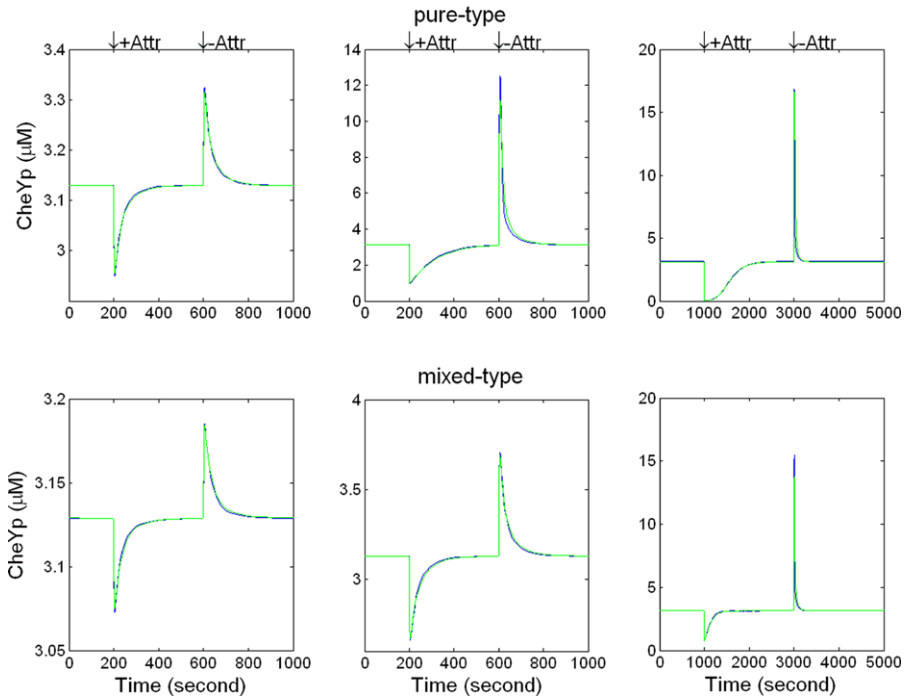
Fig. 9 Time course of CheY$_p$ in response to α-methyl-aspartate predicted by the full model (*blue line*) and the reduced model I (*green line*). In the simulations for pure-type receptors, the input is a step of α-methyl-aspartate at $t = 200$ s from 0 μM to 1 μM (*left*)/10 μM (*middle*) and thereafter a removal of the previous addition at $t = 600$ s, as well as a step at $t = 1000$ s from 0 μM to 100 μM (*right*) and thereafter a removal of the previous addition at $t = 3000$ s. In the simulations for mixed-type receptors, the input is a step of α-methyl-aspartate at $t = 200$ s from 0 μM to 1 μM (*left*)/10 μM (*middle*) and thereafter a removal of the previous addition at $t = 600$ s, as well as a step at $t = 1000$ s from 0 μM to 1000 μM (*right*) and thereafter a removal of the previous addition at $t = 3000$ s (Color figure online)

The equations that govern the evolution of the amounts of T^p, Y_p, and B_p are the same as (28)–(30). The amounts of T^a and T^i are determined by

$$T^a + T^p = T_t A, \tag{43}$$

$$T^i + T^a + T^p = T_t, \tag{44}$$

and the conservation conditions for CheY, CheZ, CheB, and CheR are the same as (32)–(34) and (40).

According to the mean-field theory, the continuum methylation level $\bar{m}$ is defined as the average methylation level of a trimer of dimers in a large receptor cluster, that is, $\bar{m} = \sum_{m=0}^{M} (\frac{m T_m}{T_t})$. The equations that govern the evolution of the amounts in the various states of the signaling trimers are as in (1)–(3). Applying the QSSA to the ligand binding reactions, the corresponding *ligand binding/release* term of the equations can be dropped, when we focus on the dynamics of slow reactions. To obtain the evolutionary equations for T_m, we sum $\frac{dT_{m,n}^s}{dt}$ over n and s. The resulting

equation set for T_m is

$$\frac{dT_m}{dt} = \begin{cases} -K_R k_{R_1} R T_0^i + K_{B_p} k_{B_3} B_p (T_1^a + T_1^p) & m = 0 \\ K_R k_{R_1} R (T_{m-1}^i - T_m^i) + K_{B_p} k_{B_3} B_p (T_{m+1}^a - T_m^a + T_{m+1}^p - T_m^p) & \\ \quad 0 < m < M \\ K_R k_{R_1} R T_{M-1}^i - K_{B_p} k_{B_3} B_p (T_M^a + T_M^p) & m = M. \end{cases} \tag{45}$$

Note that the *Activity regulation*, *Phosphorylation* and *Phosphotransfer* terms do not appear in (45). We then compute the first moment by multiplying by m and summing over m to obtain

$$\sum_{m=0}^{M} \left(m \frac{dT_m}{dt} \right) = K_R k_{R_1} R \sum_{m=0}^{M} \left[m \left(T_{m-1}^i - T_m^i \right) \right]$$

$$+ K_{B_p} k_{B_3} B_p \sum_{m=0}^{M} \left[m \left(T_{m+1}^a - T_m^a + T_{m+1}^p - T_m^p \right) \right]$$

$$= K_R k_{R_1} R \sum_{m=1}^{M} T_{m-1}^i - K_{B_p} k_{B_3} B_p \sum_{m=1}^{M} \left(T_m^a + T_m^p \right). \tag{46}$$

Since

$$\frac{d\bar{m}}{dt} = \frac{d}{dt} \sum_{m=0}^{M} \left(\frac{m T_m}{T_t} \right) = \frac{1}{T_t} \sum_{m=0}^{M} \left(m \frac{dT_m}{dt} \right),$$

we have

$$\frac{d\bar{m}}{dt} = K_R k_{R_1} R \frac{\sum_{m=1}^{M} T_{m-1}^i}{T_t} - K_{B_p} k_{B_3} B_p \frac{\sum_{m=1}^{M} (T_m^a + T_m^p)}{T_t}. \tag{47}$$

We define the average activity $A_{\bar{m}} = (\sum_{m=0}^{M}(T_m^a + T_m^p))/T_t$, that is, the fraction of the active trimers in a receptor cluster, and obviously $1 - A_{\bar{m}} = (\sum_{m=0}^{M} T_m^i)/T_t$. Comparing the definitions of $A_{\bar{m}}$ and $1 - A_{\bar{m}}$ with the terms $(\sum_{m=1}^{M}(T_m^a + T_m^p))/T_t$ and $(\sum_{m=1}^{M} T_{m-1}^i)/T_t$ in (47), we see that if we assume that the amounts of the fully methylated inactive trimers and the fully demethylated active trimers are negligible, that is $T_M^i = 0$ and $T_0^a + T_0^p = 0$, then (47) becomes

$$\frac{d\bar{m}}{dt} = K_R k_{R_1} R (1 - A_{\bar{m}}) - K_{B_p} k_{B_3} B_p A_{\bar{m}}. \tag{48}$$

This assumption is justified by the fact that methylation tends to activate receptors and demethylation tends to deactivate receptors, and that a trimer has a wide range of methylation levels and the probability of fully methylating or demethylating a trimer is low. With this assumption, we have a mean-field version of the trimer of dimers-based model. The system has only 4 differential equations to describe the signaling

behavior of a receptor trimer, whereas the full model requires 158 equations. The 4D model, which we call II, is summarized below:

$$\frac{d\bar{m}}{dt} = K_R k_{R1} R (1 - A_{\bar{m}}) - K_{B_p} k_{B3} B_p A_{\bar{m}},$$

$$\frac{dT^p}{dt} = k_A T^a - K_Y k_{Y1} Y T^p - K_B k_{B1} B T^p,$$

$$\frac{dY_p}{dt} = K_Y k_{Y1} Y T^p - k_{Y2} Y_p - K_Z k_Z Z Y_p,$$

$$\frac{dB_p}{dt} = K_B k_{B1} B T^p - k_{B2} B_p,$$

$$A_{\bar{m}} = \begin{cases} \dfrac{p_{\bar{m}}^0 + p_{\bar{m}}^1 \frac{3L}{K_{d1}^{\bar{m}}} + p_{\bar{m}}^2 \frac{3L^2}{K_{d1}^{\bar{m}} K_{d2}^{\bar{m}}} + p_{\bar{m}}^3 \frac{L^3}{K_{d1}^{\bar{m}} K_{d2}^{\bar{m}} K_{d3}^{\bar{m}}}}{1 + \frac{3L}{K_{d1}^{\bar{m}}} + \frac{3L^2}{K_{d1}^{\bar{m}} K_{d2}^{\bar{m}}} + \frac{L^3}{K_{d1}^{\bar{m}} K_{d2}^{\bar{m}} K_{d3}^{\bar{m}}}} & \text{pure-type} \\[3ex] \dfrac{p_{\bar{m}}^0 + p_{\bar{m}}^1 \frac{L}{K_{d1}^{\bar{m}}} + p_{\bar{m}}^2 \frac{2L^2}{K_{d1}^{\bar{m}} K_{d2}^{\bar{m}}} + p_{\bar{m}}^3 \frac{L^3}{K_{d1}^{\bar{m}} K_{d2}^{\bar{m}} K_{d3}^{\bar{m}}}}{1 + \frac{L}{K_{d1}^{\bar{m}}} + \frac{2L^2}{K_{d1}^{\bar{m}} K_{d2}^{\bar{m}}} + \frac{L^3}{K_{d1}^{\bar{m}} K_{d2}^{\bar{m}} K_{d3}^{\bar{m}}}} & \text{mixed-type,} \end{cases}$$

$$T_t A_{\bar{m}} = T^a + T^p,$$

$$T_t = T^i + T^a + T^p,$$

$$Y = \frac{Y_t - (1 + K_Z Z) Y_p}{1 + K_Y T^p},$$

$$Z = \frac{Z_t}{1 + K_Z Y_p},$$

$$B = \frac{B_t - [1 + K_{B_p}(T^a + T^p)] B_p}{1 + K_B T^p},$$

$$R = \frac{R_t}{1 + K_R T^i}.$$

We use the same stimulus protocol and simulate the time course of CheY$_p$ with the full system and the reduced system II, and the results are shown in Fig. 10. Clearly, the reduced system achieves perfect adaptation and captures the steady-state values of CheY$_p$ in the full system, but there is a small shift in the transient values of CheY$_p$. The time course of the reduced system consistently lags that of the full system, a discrepancy that is probably due to the linear interpolation we made for the parameters $K_{d,n}^{\bar{m}}$ and $p_{\bar{m}}^n$. Since $\bar{m}$ is defined as a continuous variable, the $\bar{m}$-dependent parameters $K_{d,n}^{\bar{m}}$ and $p_{\bar{m}}^n$ are also continuous. We assume that $K_{d,n}^{\bar{m}}$ and $p_{\bar{m}}^n$ are linear functions of $\bar{m}$, and for simplicity we used a liner interpolation between the two extreme points $\bar{m} = 0$ and $\bar{m} = M$ to estimate intermediate values. However, an examination of the discrete values of the parameters we used in the full model (Tables 3, 5, and 6) shows that both are convex functions of m, and thus they are overestimated. Thus, we used larger ligand dissociation constants and higher probabilities of being active in the simulations. The former induces a lower sensitivity, and the latter causes a higher level of CheY$_p$, which may explain the discrepancy of the two traces in Fig. 10.
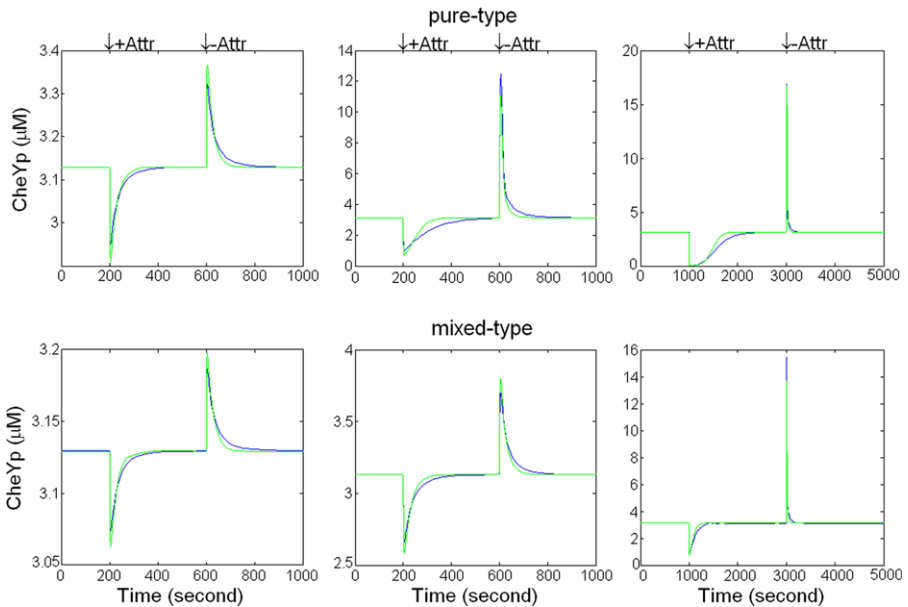
Fig. 10 Time course of CheY$_p$ in response to α-methyl-aspartate predicted by the full system (*blue line*) and the reduced system II (*green line*). In the simulations for pure-type receptors, the input is a step of α-methyl-aspartate at $t = 200$ s from 0 μM to 1 μM (*left*)/10 μM (*middle*) and thereafter a removal of the previous addition at $t = 600$ s, as well as a step at $t = 1000$ s from 0 μM to 100 μM (*right*) and thereafter a removal of the previous addition at $t = 3000$ s. In the simulations for mixed-type receptors, the input is a step of α-methyl-aspartate at $t = 200$ s from 0 μM to 1 μM (*left*)/10 μM (*middle*) and thereafter a removal of the previous addition at $t = 600$ s, as well as a step at $t = 1000$ s from 0 μM to 1000 μM (*right*) and thereafter a removal of the previous addition at $t = 3000$ s (Color figure online)

7 Discussion

The model developed here has several new aspects compared with existing models. Unlike Ising-type models, the model developed here is based on a detailed kinetic network for all known steps. We do not assume that the transition between the active and inactive states of receptors only occurs in one ligand-binding state, as in Monod et al. (1965). We are able to simulate the dynamics in the upstream pathway and analyze the cooperativity in ligand binding and kinase activity regulation that stems from receptor clustering. Using this model, we have performed sensitivity analysis and robustness tests for the full pathway, and have been able to reproduce most of the experimental observations.

Let $K_{d,n,m}^{s}$ denote the ligand dissociation constant of a receptor trimer with n ligands bound ($n = 0, \ldots, 3$), with m methyl groups added ($m = 0, \ldots, 12$), and with the activity state of s ($s = i, a, p$). A trimer of dimers undergoes a sequence of three ligand binding reactions, and this raises three key questions: (1) whether $K_{d,n,m}^{s}$ varies with m, the methylation level; (2) whether it varies with s, the receptor activity; and (3) whether it varies with n, the number of ligands bound, that is, whether cooperativity in ligand binding exists in a trimer or a larger cluster.
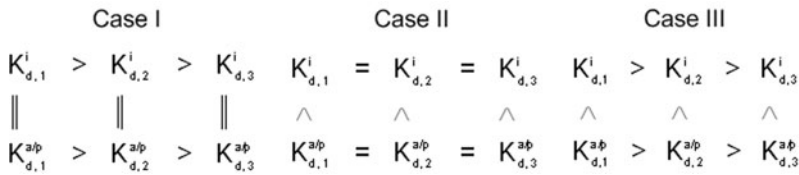
Fig. 11 Three potential patterns of chemoattractant dissociation constants of a trimer of receptor dimers. $K^i_{d,n}$ is the attractant dissociation constant of the inactive receptor trimers with n ligands bound, and $K^{a/p}_{d,n}$ is the constant of the active (unphosphorylated and phosphorylated) receptors with n ligands bound. Case I: Receptor activity has no effect on ligand affinity and positive cooperativity exists in ligand affinity. Case II: Active receptors have a lower ligand affinity and no cooperativity exists in ligand affinity. Case III: Active receptors have a lower ligand affinity and positive cooperativity exists in ligand affinity. In the figure, we only consider the effects of receptor activity and of cooperativity in ligand affinity. Dissociation constants also vary with the methylation level of receptors and the three patterns could exist for each methylation level

First, we consider the effect of the methylation level. In the model, we use a heterogeneous two-state assumption. This assumption is based on the results in Bornhorst and Falke (2003), where the authors suggest that methylation/demethylation changes the dissociation constant of inactive receptors. We assume that the variation holds for both active and inactive receptors. To test it, we perform three simulations: the first based on the assumption that only $K^{a/p}_{d,n,m}$ is heterogeneous, the second in which only $K^i_{d,n,m}$ is heterogeneous, and the third in which both are heterogeneous. It turns out that the first case cannot reproduce the experimental data (cf. Fig. 2), but the latter two can. It should be noted that the assigned parameter set is for an inhibitory ligand (α-methyl-aspartate). In this case, $K^i_{d,n,m}$ appears to dominate the apparent dissociation constant $K_{1/2}$. However, in the case of an activating ligand, by symmetry we expect that $K^{a/p}_{d,n,m}$ will dominate $K_{1/2}$, and thus the second assumption could be ruled out. Further, from the view of structural biology, the simultaneous heterogeneity of $K^i_{d,n,m}$ and $K^{a/p}_{d,n,m}$ is also feasible. As a result, it is appropriate to assume that the dissociation constant $K^s_{d,n,m}$ depends on the methylation level.

Next, we consider the effects of receptor activity and cooperativity in ligand binding jointly. For each fixed methylation level m, there are three possible patterns, as shown in Fig. 11 (for simplicity, we drop m in $K^s_{d,n,m}$). In Case I, the dissociation constant is independent of receptor activity and positive cooperativity exists in ligand affinity (the dissociation constant decreases with more ligands bound); in Case II, receptor activity lowers chemoattractant affinity (the dissociation constant of active receptors is larger than that of inactive receptors) and there is no cooperativity; and in Case III, both variations are present. With the Case II-based parameter set, we cannot capture the decay of kinase activity along with saturating concentrations of chemoattractants observed in Bornhorst and Falke's experiments (Bornhorst and Falke 2001, 2003) (data not shown). With the Case I-based parameter set (Table 3 and 5), we are able to reproduce the measures. Case III is a combination of Case I and II, and logically it cannot be ruled out. The correlation of ligand affinity and receptor activity remains to be investigated by more experimental and modeling studies.

Receptor clusters in *E. coli* have a multiple-level structural organization. It is known that two receptor monomers form a helical intertwined homodimer, and three pure-type or mixed-type dimers associate into a trimer of dimers. The trimer, together with the histidine kinase CheA and the coupling protein CheW, form a ternary signaling complex, these complexes cluster into patch in the membrane, and some patches aggregate at a cell pole. Here, we have done detailed modeling of the core structure—a trimer of dimers, and analyzed the interaction among dimer members of a trimer, which we call the *intratrimer interaction*. An extremely high Hill coefficient, as large as 11, is found in the responses of the *cheRcheB* mutant cells with Tar or Tsr highly overexpressed and by the receptor Tsr *in vitro*. This cannot be reproduced by the model for a single trimer of dimers, which suggests that the intratrimer interaction cannot account for the high cooperativity in these cases. The higher-order interaction among trimers of dimers, which we call the *intertrimer interaction*, could play a key role here. Extension of our model to a larger cluster would require estimation of a large number of parameters, most of which are not available experimentally. The existing Ising-type or MWC-type models can analyze a cluster of 10–20 receptors where a mean-field theory is applied, but the multiple-level structural organization of receptor clusters is ignored and the intratrimer and intertrimer interactions are averaged in these models. It would be useful to develop a framework that is able to model a larger receptor cluster than what we have done, but still keep the ability to explore the molecular details such as the specific roles of the intratrimer and intertrimer interactions. Investigations in this direction are in progress.

Appendix: Sensitivity Analysis

We perform sensitivity analysis for four steps of the signaling pathway—ligand binding, kinase activity regulation, phosphorylation and phosphoryl transfer in the *cheRcheB* mutant system where expression of CheR and CheB is suppressed and the methylation states of receptors are engineered and do not vary. The mutant cells can respond to but not adapt to chemoattractants. The involved chemical reactions in the system only lie in one slice (whose methylation level is the fixed one) of the network depicted in Fig. 1 excluding CheB-involved phosphoryl transfer. In the analysis, we fix the state at QEQE, and thus the reaction network lies in the $m = 6$ slice in Fig. 1 and the corresponding $m = 6$ parameter sets in Tables 1 and 3 are used in computation. For simplicity, the subindex m of the signaling complex variables is omitted in the section.

In the network, the ligand binding and kinase activity regulation transitions are much faster than autophosphorylation and phosphoryl transfer. Therefore, we apply the QSSA and dissect the network into two relatively independent parts. In the first one, we consider redistribution of signaling complexes in the ligand binding states induced by a chemoattractant stimulus. We use T_n to denote the amount of the signaling complexes with n ligands bound, regardless of the activity state ($T_n = T_n^i + T_n^a + T_n^p$).

The methylation state is fixed at QEQE and the subindex m is dropped. T_t denotes the conserved total concentration of signaling complexes. The equations that govern the evolution of the amounts in four binding states of signaling complexes are as follows:

$$\frac{dT_0}{dt} = -3k_1 L T_0 + k_{-1} T_1, \tag{49}$$

$$\frac{dT_1}{dt} = 3k_1 L T_0 - k_{-1} T_1 - 2k_2 L T_1 + 2k_{-2} T_2, \tag{50}$$

$$\frac{dT_2}{dt} = 2k_2 L T_1 - 2k_{-2} T_2 - k_3 L T_2 + 3k_{-3} T_3, \tag{51}$$

$$\frac{dT_3}{dt} = k_3 L T_2 - 3k_{-3} T_3. \tag{52}$$

The steady-state solution of ligand occupancy is

$$O = \frac{\sum_{n=0}^{3}(n T_n)}{3 T_t} = \frac{\frac{L}{K_{d1}} + \frac{2L^2}{K_{d1} K_{d2}} + \frac{L^3}{K_{d1} K_{d2} K_{d3}}}{1 + \frac{3L}{K_{d1}} + \frac{3L^2}{K_{d1} K_{d2}} + \frac{L^3}{K_{d1} K_{d2} K_{d3}}}. \tag{53}$$

We assume that when redistribution of signaling complexes in the activity states takes place, the ligand binding transitions have reached equilibrium. Then simply, $T_n^i = (1 - p_n) T_n$, and $T_n^a + T_n^P = p_n T_n$, where p_n is the probability of the signaling complex with n ligands bound being active. So, the steady-state solution of activity is

$$A = \frac{\sum_{n=0}^{3}(T_n^a + T_n^p)}{T_t} = \frac{p_0 + p_1 \frac{3L}{K_{d1}} + p_2 \frac{3L^2}{K_{d1} K_{d2}} + p_3 \frac{L^3}{K_{d1} K_{d2} K_{d3}}}{1 + \frac{3L}{K_{d1}} + \frac{3L^2}{K_{d1} K_{d2}} + \frac{L^3}{K_{d1} K_{d2} K_{d3}}}. \tag{54}$$

In the second part, we consider two slow transitions, redistribution of the active signaling complexes in the unphosphorylated and phosphorylated states, and phosphoryl transfer to CheY. We use T^i, T^a, and T^p to denote the amounts of the inactive, active-unphosphorylated and active-phosphorylated complexes, respectively, and then $T^a = \sum_{n=0}^{3} T_n^a$, $T^p = \sum_{n=0}^{3} T_n^p$, and $T_n^a + T_n^P = p_n T_n$ hold. The governing equations on T^a, T^p. and Y_p are as follows:

$$\frac{dT^a}{dt} = -k_A T^a + k_{Y1} Y T^p, \tag{55}$$

$$\frac{dT^p}{dt} = k_A T^a - k_{Y1} Y T^p, \tag{56}$$

$$\frac{dY_p}{dt} = k_{Y1} Y T^p - k_{Y2} Y^p - k_Z Z Y^p, \tag{57}$$

$$Y = Y_t - Y_p, \tag{58}$$

$$A T_t = T^a + T^p. \tag{59}$$

The steady-state solutions of T^p and Y_p are

$$T^p = \frac{n_1 A T_t - n_2 + \sqrt{\Delta}}{2n_1}, \tag{60}$$

$$Y_p = \frac{k_{Y1} Y_t T^p}{k_{Y1} T^p + k_{Y3}}, \tag{61}$$

$$k_{Y3} = k_{Y2} + k_Z Z,$$

$$n_1 = k_A k_{Y1},$$

$$n_2 = k_A k_{Y3} + k_{Y1} k_{Y3} Y_t,$$

$$n_3 = k_A k_{Y3},$$

$$\Delta = n_1^2 (A T_t)^2 + (4 n_1 n_3 - 2 n_1 n_2) A T_t + n_2^2.$$

Finally, we apply the definition of dimensionless sensitivity and obtain $S(O|L)$, $S(A|O)$, $S(T^p|A)$, and $S(Y_p|T^p)$ as Eqs. (15)–(18) in the text, respectively.

For comparison, we perform a similar analysis in the case of a signaling complex containing a receptor dimer instead of a trimer of receptor dimers. The occupancy and activity are

$$O = \frac{\frac{L}{K_{d1}}}{1 + \frac{L}{K_{d1}}}, \tag{62}$$

$$A = \frac{p_0 + p_1 \frac{L}{K_{d1}}}{1 + \frac{L}{K_{d1}}}. \tag{63}$$

The sensitivities of ligand binding and activity regulation are

$$S(O|L) = \frac{1}{1 + \frac{L}{K_{d1}}}, \tag{64}$$

$$S(A|O) = \frac{(p_1 - p_0) \frac{L}{K_{d1}}}{p_0 + p_1 \frac{L}{K_{d1}}}. \tag{65}$$

The sensitivities of the remaining steps are the same as Eqs. (17) and (18) in the text. The variation in the composition of a signaling complex does not change the formula of the downstream sensitivities, but we need adjust the values of the rate constants in the CheA related reactions due to the change in the stoichiometry of receptors and CheA, and quantitatively it would rescale the downstream sensitivities.

Using a similar technique, we perform a parametric sensitivity analysis for the upstream signaling pathway. Specially, we have interests in the sensitivities of receptor occupancy to ligand dissociation constant $S(O|K_{d_i})$ and to cooperativity in ligand affinity $S(O|t_i)$, where $t_i = K_{d_i}/K_{d_{i+1}}$ ($i = 1, 2$), and in the sensitivities of receptor activity to ligand dissociation constant $S(A|K_{d_i})$, to cooperativity in ligand affinity $S(A|t_i)$, to probability of being active $S(A|p_i)$, and to cooperativity in activity inhibition $S(A|s_i)$, where $s_i = p_{i-1}/p_i$ ($i = 1, 2, 3$). The formula are Eqs. (66)

to (82).

$$S(O|K_{d1}) = \frac{-1}{1 + \frac{3L}{K_{d1}} + \frac{3L^2}{K_{d1}K_{d2}} + \frac{L^3}{K_{d1}K_{d2}K_{d3}}}, \tag{66}$$

$$S(O|K_{d2}) = \frac{\frac{3L^2}{K_{d1}K_{d2}} + \frac{L^3}{K_{d1}K_{d2}K_{d3}}}{1 + \frac{3L}{K_{d1}} + \frac{3L^2}{K_{d1}K_{d2}} + \frac{L^3}{K_{d1}K_{d2}K_{d3}}} - \frac{\frac{2L^2}{K_{d1}K_{d2}} + \frac{L^3}{K_{d1}K_{d2}K_{d3}}}{\frac{L}{K_{d1}} + \frac{2L^2}{K_{d1}K_{d2}} + \frac{L^3}{K_{d1}K_{d2}K_{d3}}}, \tag{67}$$

$$S(O|K_{d3}) = \frac{\frac{L^3}{K_{d1}K_{d2}K_{d3}}}{1 + \frac{3L}{K_{d1}} + \frac{3L^2}{K_{d1}K_{d2}} + \frac{L^3}{K_{d1}K_{d2}K_{d3}}} - \frac{\frac{L^3}{K_{d1}K_{d2}K_{d3}}}{\frac{L}{K_{d1}} + \frac{2L^2}{K_{d1}K_{d2}} + \frac{L^3}{K_{d1}K_{d2}K_{d3}}}, \tag{68}$$

$$S(O|t_1) = \frac{\frac{2t_1L^2}{K_{d1}^2} + \frac{(3t_1 + 2t_1^2 t_2)L^3}{K_{d1}^3} + \frac{4t_1^2 t_2 L^4}{K_{d1}^4} + \frac{t_1^3 t_2 L^5}{K_{d1}^5}}{(1 + \frac{3L}{K_{d1}} + \frac{3t_1 L^2}{K_{d1}^2} + \frac{t_1^2 t_2 L^3}{K_{d1}^3})(\frac{L}{K_{d1}} + \frac{2t_1 L^2}{K_{d1}^2} + \frac{t_1^2 t_2 L^3}{K_{d1}^3})}, \tag{69}$$

$$S(O|t_2) = \frac{\frac{t_1^2 t_2 L^3}{K_{d1}^3} + \frac{2t_1^2 t_2 L^4}{K_{d1}^4} + \frac{t_1^3 t_2 L^5}{K_{d1}^5}}{(1 + \frac{3L}{K_{d1}} + \frac{3t_1 L^2}{K_{d1}^2} + \frac{t_1^2 t_2 L^3}{K_{d1}^3})(\frac{L}{K_{d1}} + \frac{2t_1 L^2}{K_{d1}^2} + \frac{t_1^2 t_2 L^3}{K_{d1}^3})}, \tag{70}$$

$$S(A|p_0) = \frac{p_0}{p_0 + p_1 \frac{3L}{K_{d1}} + p_2 \frac{3L^2}{K_{d1}K_{d2}} + p_3 \frac{L^3}{K_{d1}K_{d2}K_{d3}}}, \tag{71}$$

$$S(A|p_1) = \frac{p_1 \frac{3L}{K_{d1}}}{p_0 + p_1 \frac{3L}{K_{d1}} + p_2 \frac{3L^2}{K_{d1}K_{d2}} + p_3 \frac{L^3}{K_{d1}K_{d2}K_{d3}}}, \tag{72}$$

$$S(A|p_2) = \frac{p_2 \frac{3L^2}{K_{d1}K_{d2}}}{p_0 + p_1 \frac{3L}{K_{d1}} + p_2 \frac{3L^2}{K_{d1}K_{d2}} + p_3 \frac{L^3}{K_{d1}K_{d2}K_{d3}}}, \tag{73}$$

$$S(A|p_3) = \frac{p_3 \frac{L^3}{K_{d1}K_{d2}K_{d3}}}{p_0 + p_1 \frac{3L}{K_{d1}} + p_2 \frac{3L^2}{K_{d1}K_{d2}} + p_3 \frac{L^3}{K_{d1}K_{d2}K_{d3}}}, \tag{74}$$

$$S(A|s_1) = -\frac{\frac{1}{s_1}\frac{3L}{K_{d1}} + \frac{1}{s_1 s_2}\frac{3L^2}{K_{d1}K_{d2}} + \frac{1}{s_1 s_2 s_3}\frac{L^3}{K_{d1}K_{d2}K_{d3}}}{1 + \frac{1}{s_1}\frac{3L}{K_{d1}} + \frac{1}{s_1 s_2}\frac{3L^2}{K_{d1}K_{d2}} + \frac{1}{s_1 s_2 s_3}\frac{L^3}{K_{d1}K_{d2}K_{d3}}}, \tag{75}$$

$$S(A|s_2) = -\frac{\frac{1}{s_1 s_2}\frac{3L^2}{K_{d1}K_{d2}} + \frac{1}{s_1 s_2 s_3}\frac{L^3}{K_{d1}K_{d2}K_{d3}}}{1 + \frac{1}{s_1}\frac{3L}{K_{d1}} + \frac{1}{s_1 s_2}\frac{3L^2}{K_{d1}K_{d2}} + \frac{1}{s_1 s_2 s_3}\frac{L^3}{K_{d1}K_{d2}K_{d3}}}, \tag{76}$$

$$S(A|s_3) = -\frac{\frac{1}{s_1 s_2 s_3}\frac{L^3}{K_{d1}K_{d2}K_{d3}}}{1 + \frac{1}{s_1}\frac{3L}{K_{d1}} + \frac{1}{s_1 s_2}\frac{3L^2}{K_{d1}K_{d2}} + \frac{1}{s_1 s_2 s_3}\frac{L^3}{K_{d1}K_{d2}K_{d3}}}, \tag{77}$$

$$S(A|K_{d1}) = \frac{\frac{3L}{K_{d1}} + \frac{3L^2}{K_{d1}K_{d2}} + \frac{L^3}{K_{d1}K_{d2}K_{d3}}}{1 + \frac{3L}{K_{d1}} + \frac{3L^2}{K_{d1}K_{d2}} + \frac{L^3}{K_{d1}K_{d2}K_{d3}}}$$
$$- \frac{p_1\frac{3L}{K_{d1}} + p_2\frac{3L^2}{K_{d1}K_{d2}} + p_3\frac{L^3}{K_{d1}K_{d2}K_{d3}}}{p_0 + p_1\frac{3L}{K_{d1}} + p_2\frac{3L^2}{K_{d1}K_{d2}} + p_3\frac{L^3}{K_{d1}K_{d2}K_{d3}}}, \tag{78}$$

$$S(A|K_{d2}) = \frac{\frac{3L^2}{K_{d1}K_{d2}} + \frac{L^3}{K_{d1}K_{d2}K_{d3}}}{1 + \frac{3L}{K_{d1}} + \frac{3L^2}{K_{d1}K_{d2}} + \frac{L^3}{K_{d1}K_{d2}K_{d3}}}$$
$$- \frac{p_2\frac{3L^2}{K_{d1}K_{d2}} + p_3\frac{L^3}{K_{d1}K_{d2}K_{d3}}}{p_0 + p_1\frac{3L}{K_{d1}} + p_2\frac{3L^2}{K_{d1}K_{d2}} + p_3\frac{L^3}{K_{d1}K_{d2}K_{d3}}}, \tag{79}$$

$$S(A|K_{d3}) = \frac{\frac{L^3}{K_{d1}K_{d2}K_{d3}}}{1 + \frac{3L}{K_{d1}} + \frac{3L^2}{K_{d1}K_{d2}} + \frac{L^3}{K_{d1}K_{d2}K_{d3}}}$$
$$- \frac{p_3\frac{L^3}{K_{d1}K_{d2}K_{d3}}}{p_0 + p_1\frac{3L}{K_{d1}} + p_2\frac{3L^2}{K_{d1}K_{d2}} + p_3\frac{L^3}{K_{d1}K_{d2}K_{d3}}}, \tag{80}$$

$$S(A|t_1) = \frac{p_2\frac{3t_1L^2}{K_{d1}^2} + p_3\frac{2t_1^2t_2L^3}{K_{d1}^3}}{p_0 + p_1\frac{3L}{K_{d1}} + p_2\frac{3L^2}{K_{d1}^2} + p_3\frac{t_1^2t_2L^3}{K_{d1}^3}} - \frac{\frac{3t_1L^2}{K_{d1}^2} + \frac{2t_1^2t_2L^3}{K_{d1}^3}}{1 + \frac{3L}{K_{d1}} + \frac{3t_1L^2}{K_{d1}^2} + \frac{t_1^2t_2L^3}{K_{d1}^3}}, \tag{81}$$

$$S(A|t_2) = \frac{p_3\frac{t_1^2t_2L^3}{K_{d1}^3}}{p_0 + p_1\frac{3L}{K_{d1}} + p_2\frac{3t_1L^2}{K_{d1}^2} + p_3\frac{t_1^2t_2L^3}{K_{d1}^3}} - \frac{\frac{t_1^2t_2L^3}{K_{d1}^3}}{1 + \frac{3L}{K_{d1}} + \frac{3t_1L^2}{K_{d1}^2} + \frac{t_1^2t_2L^3}{K_{d1}^3}}. \tag{82}$$

References

Albert, R., Chiu, Y., & Othmer, H. G. (2004). Dynamic receptor team formation can explain the high signal transduction gain in *Escherichia coli*. *Biophys. J.*, *86*(5), 2650–2659.

Alon, U., Camarena, L., Surette, M. G., Arcas, B. A., Liu, Y., Leibler, S., & Stock, J. B. (1998). Response regulator output in bacterial chemotaxis. *EMBO J.*, *17*, 4238–4248.

Alon, U., Surette, M. G., Barkai, N., & Leibler, S. (1999). Robustness in bacterial chemotaxis. *Nature*, *15*, 168–171.

Ames, P., Studdert, C. A., Reiser, R. H., & Parkinson, J. S. (2002). Collaborative signaling by mixed chemoreceptor teams in *Escherichia coli*. *Proc. Natl Acad. Sci.*, *99*(10), 7060.

Barkai, N., & Leibler, S. (1997). Robustness in simple biochemical networks. *Nature*, *387*(6636), 913–917.

Berg, H. C. (1975). How bacteria swim. *Sci. Am.*, *233*, 36–44.

Berg, H. C., & Brown, D. A. (1972). Chemotaxis in *Escherichia coli* analysed by three-dimensional tracking. *Nature*, *239*(5374), 500–504.

Berg, H. C., & Tedesco, P. M. (1975). Transient response to chemotactic stimuli in *Escherichia coli*. *Proc. Natl Acad. Sci.*, *72*(8), 3235–3239.

Bjorkman, A. M., Dunten, P., Sandgren, M. O. J., Dwarakanath, V. N., & Mowbray, S. L. (2001). Mutations that affect ligand binding to the *Escherichia coli* aspartate receptor. *J. Biol. Chem.*, *276*(4), 2808–2815.

Block, S. M., Segall, J. E., & Berg, H. C. (1982). Impulse responses in bacterial chemotaxis. *Cell*, *31*(1), 215–226.

Boldog, T., Grimme, S., Li, M., Sligar, S. G., & Hazelbauer, G. L. (2006). Nanodiscs separate chemoreceptor oligomeric states and reveal their signaling properties. *Proc. Natl Acad. Sci.*, *103*(31), 11509.

Borkovich, K. A., Alex, L. A., & Simon, M. I. (1992). Attenuation of sensory receptor signaling by covalent modification. *Proc. Natl Acad. Sci.*, *89*(15), 6756–6760.

Bornhorst, J. A., & Falke, J. J. (2001). Evidence that both ligand binding and covalent adaptation drive a two-state equilibrium in the aspartate receptor signaling complex. *J. Gen. Physiol.*, *118*(6), 693–710.

Bornhorst, J. A., & Falke, J. J. (2003). Quantitative analysis of aspartate receptor signaling complex reveals that the homogeneous two-state model is inadequate: development of a heterogeneous two-state model. *J. Mol. Biol.*, *326*(5), 1597–1614.

Bourret, R. B., & Stock, A. M. (2002). Molecular information processing: lessons from bacterial chemotaxis. *J. Biol. Chem.*, *277*(12), 9625–9628.

Bourret, R. B., Borkovich, K. A., & Simon, M. I. (1991). Signal transduction pathways involving protein phosphorylation in prokaryotes. *Annu. Rev. Biochem.*, *60*(1), 401–441.

Boyd, A., & Simon, M. I. (1980). Stimulus-induced methylation generates multiple electrophoretic forms of methyl-accepting chemotaxis proteins in *Escherichia coli*. *J. Bacteriol.*, *143*, 809–815.

Bray, D., Levin, M. D., & Morton-Firth, C. J. (1998). Receptor clustering as a cellular mechanism to control sensitivity. *Nature*, *393*(6680), 85–88.

Briegel, A., Ding, H. J., Li, Z., Werner, J., Gitai, Z., Dias, D. P., Jensen, R. B., & Jensen, G. J. (2008). Location and architecture of the *Caulobacter crescentus* chemoreceptor array. *Mol. Microbiol.*, *69*(1), 30–41.

Briegel, A., Ortega, D. R., Tocheva, E. I., Wuichet, K., Li, Z., Chen, S., Müller, A., Iancu, C. V., Murphy, G. E., Dobro, M. J., et al. (2009). Universal architecture of bacterial chemoreceptor arrays. *Proc. Natl Acad. Sci.*, *106*(40), 17181–17186.

Cardozo, M. J., Massazza, D. A., Parkinson, J. S., & Studdert, C. A. (2010). Disruption of chemoreceptor signalling arrays by high levels of chew, the receptor–kinase coupling protein. *Mol. Microbiol.*, *75*(5), 1171–1181.

Duke, T. A. J., & Bray, D. (1999). Heightened sensitivity of a lattice of membrane receptors. *Proc. Natl Acad. Sci.*, *96*(18), 10104–10108.

Endres, R. G., & Wingreen, N. S. (2006). Precise adaptation in bacterial chemotaxis through "assistance neighborhoods". *Proc. Natl Acad. Sci.*, *103*(35), 13040.

Endres, R. G., Falke, J. J., & Wingreen, N. S. (2007). Chemotaxis receptor complexes: from signaling to assembly. *PLoS Comput. Biol.*, *3*(7), 1385–1393.

Francis, N. R., Levit, M. N., Shaikh, T. R., Melanson, L. A., Stock, J. B., & DeRosier, D. J. (2002). Subunit organization in a soluble complex of Tar, CheW, and CheA by electron microscopy. *J. Biol. Chem.*, *277*(39), 36755–36759.

Francis, N. R., Wolanin, P. M., Stock, J. B., DeRosier, D. J., & Thomas, D. R. (2004). Three-dimensional structure and organization of a receptor/signaling complex. *Proc. Natl Acad. Sci.*, *101*(50), 17480–17485.

Heinrich, R., Schuster, S., & Holzhutter, H. G. (1991). Mathematical analysis of enzymic reaction systems using optimization principles. *Eur. J. Biochem.*, *201*(1), 1–21.

Keymer, J. E., Endres, R. G., Skoge, M., Meir, Y., & Wingreen, N. S. (2006). Chemosensing in *Escherichia coli*: two regimes of two-state receptors. *Proc. Natl Acad. Sci.*, *103*(6), 1786–1791.

Khursigara, C. M., Wu, X., & Subramaniam, S. (2008). Chemoreceptors in *Caulobacter crescentus*: trimers of receptor dimers in a partially ordered hexagonally packed array. *J. Bacteriol.*, *190*(20), 6805–6810.

Kim, K. K., Yokota, H., & Kim, S. H. (1999). Four-helical-bundle structure of the cytoplasmic domain of a serine chemotaxis receptor. *Nature*, *400*(6746), 787.

Kollmann, M., Loevdok, L., Bartholome, K., Timmer, J., & Sourjik, V. (2005). Design principles of a bacterial signalling network. *Nature*, *438*(7067), 504–507.

Koshland, D. E. (1980). *Bacterial chemotaxis as a model behavioral system*. New York: Raven Press.

Larsen, S. H., Reader, R. W., Kort, E. N., Tso, W. W., & Adler, J. (1974). Change in direction of flagellar rotation is the basis of the chemotactic response in *Escherichia coli*. *Nature*, *249*(5452), 74–77.

Lee, C. H., & Othmer, H. G. (2010). A multi-time-scale analysis of chemical reaction networks: I. Deterministic systems. *J. Math. Biol.*, *60*(3), 387–450.

Levit, M. N., & Stock, J. B. (2002). Receptor methylation controls the magnitude of stimulus-response coupling in bacterial chemotaxis. *J. Biol. Chem.*, *277*(39), 36760–36765.

Levit, M. N., Grebe, T. W., & Stock, J. B. (2002). Organization of the receptor-kinase signaling array that regulates *Escherichia coli* chemotaxis. *J. Biol. Chem.*, *277*(39), 36748–36754.

Li, M., & Hazelbauer, G. L. (2004). Cellular stoichiometry of the components of the chemotaxis signaling complex. *J. Bacteriol.*, *186*(12), 3687–3694.

Li, G., & Weis, R. M. (2000). Covalent modification regulates ligand binding to receptor complexes in the chemosensory system of *Escherichia coli*. *Cell*, *100*(3), 357–365.

Li, J., Swanson, R. V., Simon, M. I., & Weis, R. M. (1995). Response regulators CheB and CheY exhibit competitive binding to the kinase CheA. *Biochemistry*, *34*(45), 14626–14636.

Liberman, L., Berg, H. C., & Sourjik, V. (2004). Effect of chemoreceptor modification on assembly and activity of the receptor-kinase complex in *Escherichia coli*. *J. Bacteriol.*, *186*(19), 6643–6646.

Liu, Y., Levit, M., Lurz, R., Surette, M. G., & Stock, J. B. (1997). Receptor-mediated protein kinase activation and the mechanism of transmembrane signaling in bacterial chemotaxis. *EMBO J.*, *16*(24), 7231.

Lřvdok, L., Kollmann, M., & Sourjik, V. (2007). Co-expression of signaling proteins improves robustness of the bacterial chemotaxis pathway. *J. Biotechnol.*, *129*(2), 173–180.

Maddock, J. R., & Shapiro, L. (1993). Polar location of the chemoreceptor complex in the *Escherichia coli* cell. *Science*, *259*(5102), 1717–1723.

Mello, B. A., & Tu, Y. (2003). Quantitative modeling of sensitivity in bacterial chemotaxis: the role of coupling among different chemoreceptor species. *Proc. Natl Acad. Sci.*, *100*(14), 8223–8228.

Mello, B. A., & Tu, Y. (2005). An allosteric model for heterogeneous receptor complexes: understanding bacterial chemotaxis responses to multiple stimuli. *Proc. Natl Acad. Sci.*, *102*(48), 17354–17359.

Mello, B. A., Shaw, L., & Tu, Y. (2004). Effects of receptor interaction in bacterial chemotaxis. *Biophys. J.*, *87*(3), 1578–1595.

Monod, J., Wyman, J., & Changeux, J. P. (1965). On the nature of allosteric transitions: a plausible model. *J. Mol. Biol.*, *12*, 88–118.

Morton-Firth, C. J., Shimizu, T. S., & Bray, D. (1999). A free-energy-based stochastic simulation of the Tar receptor complex. *J. Mol. Biol.*, *286*(4), 1059–1074.

Ninfa, E. G., Stock, A., Mowbray, S., & Stock, J. (1991). Reconstitution of the bacterial chemotaxis signal transduction system from purified components. *J. Biol. Chem.*, *266*(15), 9764–9770.

Park, M. J., Dahlquist, F. W., & Doyle, F. J. III (2007). Simultaneous high gain and wide dynamic range in a model of bacterial chemotaxis. *IET Syst. Biol.*, *1*(4), 222–229.

Rao, C. V., Frenklach, M., & Arkin, A. P. (2004a). An allosteric model for transmembrane signaling in bacterial chemotaxis. *J. Mol. Biol.*, *343*(2), 291–303.

Rao, C. V., Kirby, J. R., & Arkin, A. P. (2004b). Design and diversity in bacterial chemotaxis: a comparative study in *Escherichia coli* and *Bacillus subtilis*. *PLoS Biol.*, *2*, 239–252.

Scharf, B. E., Fahrner, K. A., Turner, L., & Berg, H. C. (1998). Control of direction of flagellar rotation in bacterial chemotaxis. *Proc. Natl Acad. Sci.*, *95*(1), 201–206.

Segall, J. E., Block, S. M., & Berg, H. C. (1986). Temporal comparisons in bacterial chemotaxis. *Proc. Natl Acad. Sci.*, *83*(23), 8987–8991.

Shi, Y., & Duke, T. (1998). Cooperative model of bacterial sensing. *Phys. Rev. E*, *58*(5), 6399–6406.

Shimizu, T. S., Aksenov, S. V., & Bray, D. (2003). A spatially extended stochastic model of the bacterial chemotaxis signalling pathway. *J. Mol. Biol.*, *329*(2), 291–309.

Silverman, M., & Simon, M. (1974). Flagellar rotation and the mechanism of bacterial motility. *Nature*, *249*(5452), 73–74.

Silversmith, R. E., Smith, J. G., Guanga, G. P., Les, J. T., & Bourret, R. B. (2001). Alteration of a non-conserved active site residue in the chemotaxis response regulator CheY affects phosphorylation and interaction with CheZ. *J. Biol. Chem.*, *276*(21), 18478–18484.

Simms, S. A., Keane, M. G., & Stock, J. (1985). Multiple forms of the CheB methylesterase in bacterial chemosensing. *J. Biol. Chem.*, *260*(18), 10161–10168.

Simms, S. A., Stock, A. M., & Stock, J. B. (1987). Purification and characterization of the S-adenosylmethionine: glutamyl methyltransferase that modifies membrane chemoreceptor proteins in bacteria. *J. Biol. Chem.*, *262*(18), 8537–8543.

Sourjik, V., & Berg, H. C. (2002a). Receptor sensitivity in bacterial chemotaxis. *Proc. Natl Acad. Sci.*, *99*(1), 123–127.

Sourjik, V., & Berg, H. C. (2002b). Binding of the *Escherichia coli* response regulator CheY to its target measured *in vivo* by fluorescence resonance energy transfer. *Proc. Natl Acad. Sci.*, *99*(20), 12669–12674.

Sourjik, V., & Berg, H. C. (2004). Functional interactions between receptors in bacterial chemotaxis. *Nature*, *428*(6981), 437–441.

Spiro, P. A., Parkinson, J. S., & Othmer, H. G. (1997). A model of excitation and adaptation in bacterial chemotaxis. *Proc. Natl Acad. Sci.*, *94*(14), 7263–7268.

Spudich, J. L., & Koshland, D. E. (1975). Quantitation of the sensory response in bacterial chemotaxis. *Proc. Natl Acad. Sci.*, *72*(2), 710–713.

Starrett, D. J., & Falke, J. J. (2005). Adaptation mechanism of the aspartate receptor: electrostatics of the adaptation subdomain play a key role in modulating kinase activity. *Biochemistry*, *44*(5), 1550.

Stewart, R. C., Jahreis, K., & Parkinson, J. S. (2000). Rapid phosphotransfer to CheY from a CheA protein lacking the CheY-binding domain. *Biochemistry*, *39*(43), 13157–13165.

Stock, J. B. (1994). *Regulation of cellular signal transduction pathways by desensitization and amplification*. New York: Wiley.

Stock, J. B., Lukat, G. S., & Stock, A. M. (1991). Bacterial chemotaxis and the molecular logic of intracellular signal transduction networks. *Annu. Rev. Biophys. Biophys. Chem.*, *20*(1), 109–136.

Studdert, C. A., & Parkinson, J. S. (2004). Crosslinking snapshots of bacterial chemoreceptor squads. *Proc. Natl Acad. Sci.*, *101*(7), 2117–2122.

Studdert, C. A., & Parkinson, J. S. (2005). Insights into the organization and dynamics of bacterial chemoreceptor clusters through *in vivo* crosslinking studies. *Proc. Natl Acad. Sci.*, *102*(43), 15623–15628.